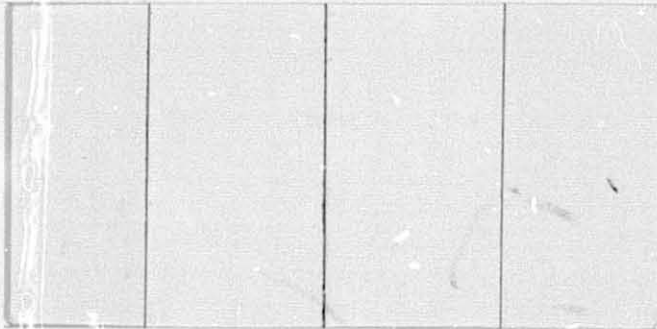
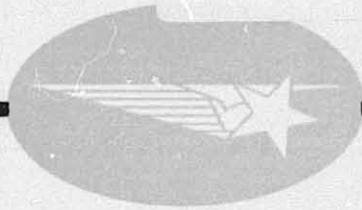


General Disclaimer

One or more of the Following Statements may affect this Document

- This document has been reproduced from the best copy furnished by the organizational source. It is being released in the interest of making available as much information as possible.
- This document may contain data, which exceeds the sheet parameters. It was furnished in this condition by the organizational source and is the best copy available.
- This document may contain tone-on-tone or color graphs, charts and/or pictures, which have been reproduced in black and white.
- This document is paginated as submitted by the original source.
- Portions of this document are not fully legible due to the historical nature of some of the material. However, it is the best reproduction available from the original submission.



terminal

(NASA-CR-144036) SKYLAB M518 MULTIPURPOSE
FURNACE CONVECTION ANALYSIS Final Report
(Lockheed Missiles and Space Co.) 85 p
HC \$5.00

N76-11882

CSCI 20B

Unclas
G3/76 01581

Lockheed

Missiles & Space Company, Inc.

HUNTSVILLE RESEARCH & ENGINEERING CENTER

Cummings Research Park
4800 Bradford Drive,
Huntsville, Alabama

**SKYLAB M518 MULTIPURPOSE
FURNACE CONVECTION ANALYSIS**

FINAL REPORT

September 1975

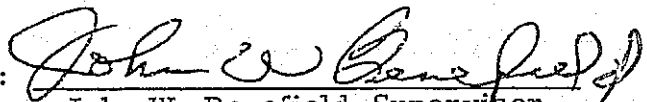
Contract NAS8-27015

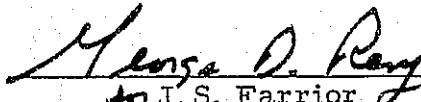
Prepared for National Aeronautics and Space Administration
Marshall Space Flight Center, Alabama 35812

by

S. V. Bourgeois
L. W. Spradley

APPROVED:


John W. Benefield, Supervisor
Advanced Technology Systems Section


J. S. Farrior
Resident Director

FOREWORD

This report was prepared for the National Aeronautics and Space Administration, Marshall Space Flight Center, as a final report on Contract NAS8-27015. This report describes an evaluation of natural convection in the microgravity of Skylab and its effects on space processing experiments M556, M559, M560 and M562. The work was performed in the Space Processing Group of the Lockheed-Huntsville Research & Engineering Center.

The NASA Contracting Officer's Representative was B. R. Facemire, MSFC Space Science Laboratory.

ACKNOWLEDGMENT

The effort of Dr. J. P. Doty in compiling Appendix B is hereby gratefully acknowledged. The authors also extend their appreciation to Mr. Tommy Bannister of MSFC, to Dr. P. G. Grodzka of Lockheed-Huntsville, to Dr. H. U. Walters, University of Alabama, and to Dr. Heribert H. Wiedemeier of Rensselaer Polytechnic Institute for their helpful comments and advice throughout the period of this investigation.

CONTENTS

Section		Page
	FOREWORD	ii
1	INTRODUCTION AND SUMMARY	1
2	CONVECTION SENSITIVITY	3
	2.1 Thermogravitational Dimensional Analysis	3
	2.2 Thermocapillary Dimensional Analysis	6
	2.3 Heat and Mass Transfer Rates	9
	2.4 Conclusions	10
3	COMPUTER PROGRAM MODELS	11
	3.1 LOCAP	11
	3.2 Methodology of Computer Models	12
	3.3 GeI ₄ Model Results	13
	3.4 InSb Model Results	22
	3.5 Germanium Cases	49
	3.6 Summary of Conclusions	53
4	COMPARISON OF EXPERIMENTAL AND THEORETICAL RESULTS	55
	4.1 GeI ₄ Experiment	55
	4.2 M560 InSb Experiment	56
	4.3 M562 InSb Experiment	57
	4.4 M559 Germanium Experiment	58
5	CONCLUSIONS AND RECOMMENDATIONS	59
6	REFERENCES	61
7	NOMENCLATURE	63

Appendix		Page
A	Description of Lockheed Convection Analysis Program LOCAP	A-1
B	InSb Oxide Films	B-1
C	Dopant Effect on Melt-Vapor Surface Tension	C-1

Section 1
INTRODUCTION AND SUMMARY

At the request of the principal investigators for Skylab experiments M556 "Vapor Growth of IV-VI Compounds" (H. Wiedemeier, Rensselaer Polytechnic Institute) and M560 "Growth of Spherical Crystals" (H. U. Walters, University of Alabama in Huntsville), an analysis was performed of the convection which existed on ground tests and during Skylab processing of these experiments. A parallel analysis was also performed on Skylab experiment M562 "Indium Antimonide Crystals" (H. Gatos, Massachusetts Institute of Technology) because indium antimonide (InSb) was used and a free surface existed in the tellurium-doped Skylab III sample. In addition, brief analyses were also performed of the M559 "Microsegregation in Germanium" (J. T. Yue, Texas Instruments) because the Skylab crystals indicated turbulent convection effects.

By utilizing simple dimensional analysis calculations or a more accurate, but complex, convection computer model, it is shown that:

- Neither thermogravitational, g-jitter or thermoacoustic convection can account for the unexpected, order-of-magnitude increase in mass transport rate observed in GeI_4 experiment M556, Skylab Case 3A.
- Turbulent convection existing during Skylab experiment M559 "Microsegregation in Germanium" was definitely caused by thermocapillary forces as predicted from theory both by dimensional analysis and by a convection model.
- From theoretical considerations, both indium-antimonide experiments M560 and M562 should have exhibited substantial thermocapillary convection, but did not due to probable oxide film interference (or opposing solutal effects).

The most important, and baffling, of these results is the rather obvious conflict between experiment and theory for the indium-antimonide experiments.

The correct explanation for the suppression of thermocapillary convection in these space grown, melt crystals is critically important because it could lead to containerless, diffusion controlled growth of such important materials as silicon, germanium and aluminum oxide. It is baffling because theory so strongly predicts significant thermocapillary convection (Marangoni numbers greater than 1000), yet the apparent lack of convective effects in the space grown crystals is also strongly evident. It is also paradoxical because of the agreement between experimental evidence and theory for the germanium experiment.

It should be noted that no significant deficiencies exist in the theory or analysis techniques utilized in assessing the M560 and M562 experiments. It is, however, the lack of data on physical properties (see Appendices B and C) and the rather limited time and resources allotted to this assessment which do not presently allow the complete resolution of the conflicting experimental and theoretical results.

By conducting the preceding analysis, it has been shown that rigorous convection sensitivity and/or convection modeling analyses, in conjunction with measurement or prediction of capillary effects, need to be applied to all space processing flight experiments before final designs are chosen if convection suppression is desired.

The following sections contain descriptions of: dimensional analysis utilized to estimate convection expected on Earth versus Skylab; results of computer program models to determine convective flow patterns and heat and mass transport rates; comparison of theoretical and experimental results; and recommendations of further work required to resolve the present difference in experimental and theoretical results.

Section 2

CONVECTION SENSITIVITY

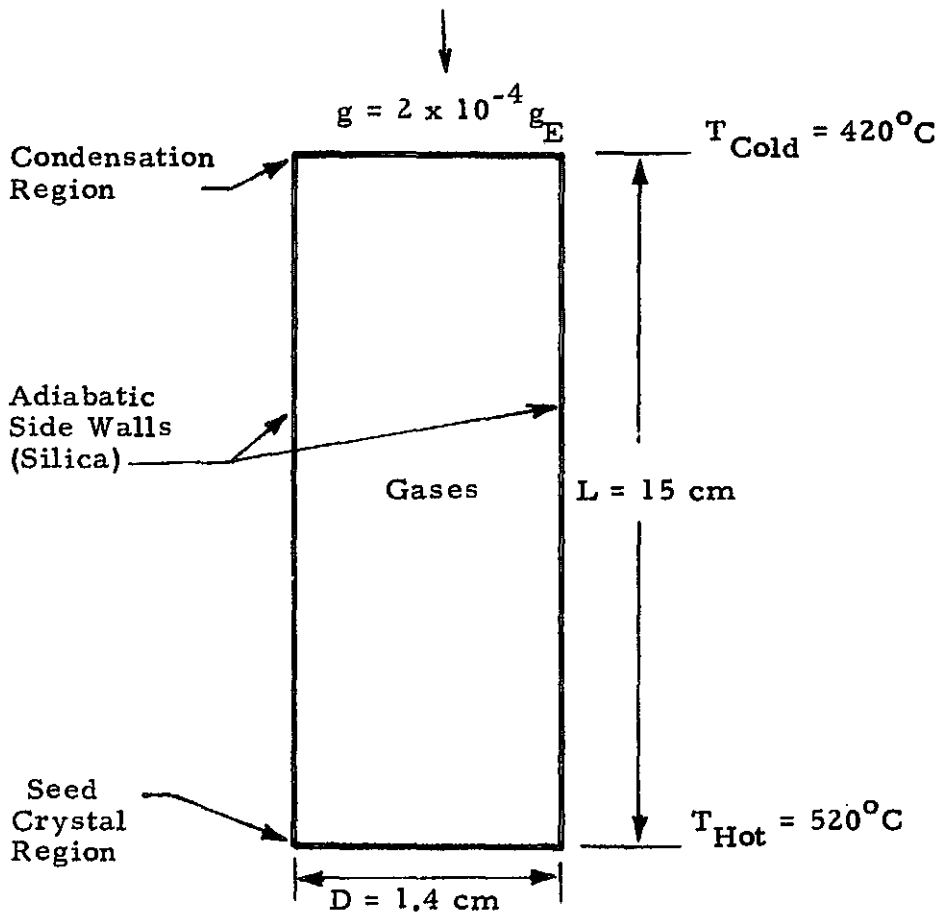
A simple, reliable estimate of whether convection exists, and its strength, can be obtained from dimensional analysis. This is especially true for thermogravitational flows which have been studied extensively (both theoretically and experimentally) for the past 30 years (Ref. 1). The analysis of thermocapillary flows, however, is not as extensive due to the difficulty of suppressing the usually dominant buoyancy forces during terrestrial experiments. The following sections describe: an analysis of the magnitude of thermogravitational convection expected in Skylab and ground testing; thermocapillary convection expected in Skylab; and a means for estimating mass transfer effects via heat and mass transfer analogies.

2.1 Thermogravitational Dimensional Analysis

A schematic of the M556 GeI₄ process is shown in Fig. 1. The pressure of the GeI₄ gas was determined by utilizing an ideal gas and the mean temperature in the container (470°C). A schematic typical of the M560 and M562 InSb processes are shown in Fig. 2. Dimensional analysis of these configurations requires that values of the Rayleigh and Marangoni numbers be calculated for both terrestrial and Skylab conditions and then compared to the critical Rayleigh and Marangoni numbers. The aspect ratio (length-to-diameter) and Prandtl number of the processes are also important parameters. Ignoring the Marangoni effect for the present, the dimensional analysis for buoyancy convection is presented in this section.

o GeI₄ Experiment

For heating from below or above (vertical processing) the Rayleigh number is defined as:



$$P \{ \text{Ge I}_4(g) \} = 1.5 \text{ atm}$$

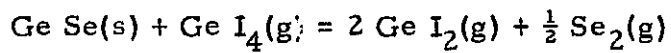


Fig. 1 - Skylab M556 Ge I_4 Processing Parameters

$$Ra_L = \beta g \frac{(T_{Hot} - T_{Cold}) L^3}{\nu \alpha}$$

where

β = thermal expansion coefficient ($1.35 \cdot 10^{-3}/^{\circ}C$)

g = gravity level (cm/sec^2)

ν = kinematic viscosity ($1.6 \cdot 10^{-2} cm^2/sec$)

α = thermal diffusivity ($1.35 \cdot 10^{-2} cm^2/sec$)

The mean gravity during Skylab 3 was approximately $2 \cdot 10^{-4} g_E$ ($g_E = 980 cm/sec^2$). Thus during vertical processing, $Ra \downarrow_{Earth} = 2 \cdot 10^9$ and $Ra \downarrow_{Skylab} = 4 \cdot 10^5$. The critical Rayleigh number, Ra_L^C , depends on the heating direction, aspect ratio (γ), and Prandtl number (Pr). For the M556 experiment, $Pr = 1.2$ and $\gamma = L/D = 11$. Thus $Ra_L^C = 2 \cdot 10^6$ for heating from below (Ref. 2) and convection is probable only in ground processing. $Ra_L^C = \infty$ for heating from above which means that convection is theoretically always absent. In reality, however, finite lateral temperature gradients exist (side heating or cooling); and Ra for side heating is zero (some flow always exists). In side heating, however, the heat and mass transport may not be increased until a second critical Rayleigh number, Ra_w^C , is reached.

For side heating (horizontal processing) the Rayleigh number is defined as.

$$Ra_w = g (T_{Hot} - T_{Cold}) D^3 / T_{Mean} \nu \alpha$$

and the critical Rayleigh number for convective heat and mass transport is defined as (Ref. 3).

$$Ra_w^C = 592 \gamma \sqrt{\gamma - 1} = 2 \cdot 10^4$$

For ground processing, $Ra_w = 1.6 \cdot 10^6$; while for Skylab, $Ra_w = 3 \cdot 2 \cdot 10^2$. Thus convection is not expected to influence heat and mass transport on Skylab if gravity is oriented perpendicular to the direction of the temperature gradient. but it will influence horizontal ground processing significantly.

o InSb Experiment

The Prandtl number and aspect ratios for the configuration of Fig. 2 are:

$$Pr = 0.01$$

$$\gamma = 4.00$$

Thus the critical numbers are $Ra_L^c = 2 \times 10^5$ (Ref. 2) and $Ra_w^c = 4 \times 10^3$ (Ref. 3). Utilizing a Skylab mean gravity level of $2.10^{-4} g_E$, the Rayleigh numbers are:

	<u>Ground</u>	<u>Skylab</u>
Ra_L/Ra_L^c	81	8×10^{-3}
Ra_w/Ra_w^c	371	4×10^{-2}

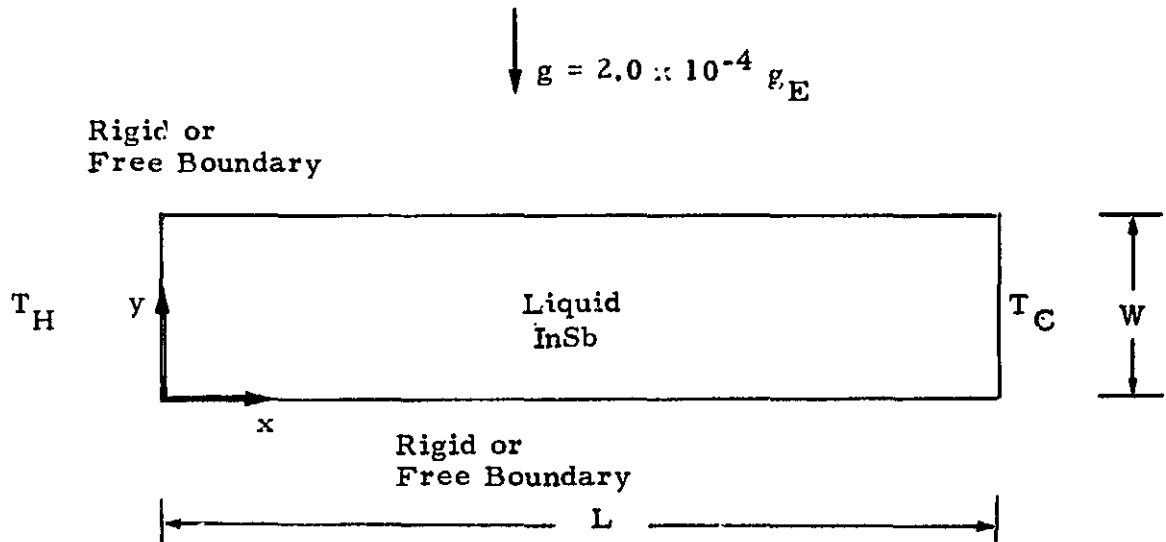
Thus, as for the GeI_4 experiment, convection is likely during heating from below processing on the ground but not on Skylab; while horizontal processing will yield convective influences during ground processing, but on Skylab, little or no convective heat or mass transport will exist (although finite motion will arise).

o Computer Model Analysis

The preceding dimensional analysis suggests that appreciable convection is not predicted to exist during Skylab processing from buoyancy forces. To precisely determine the magnitude of convection and flow patterns, the Lockheed Convection Analysis Computer program is utilized in Section 3 to quantitatively assess thermogravitational flows.

2.2 THERMOCAPILLARY DIMENSIONAL ANALYSIS

Surface tension gradients may be an important source of convection in crystal growth whenever a liquid-fluid interface is present (Ref. 4). Since no such interfaces exist in the M556 GeI_4 experiment, only the InSb experiments will be analyzed. Furthermore, solutocapillary convection will be ignored due



Thermal Conditions:

$$T_C = 537^\circ\text{C}$$

$$T_H = 780^\circ\text{C}$$

Insulated Top and Bottom Walls

Dimensions:

$$L = 6.0 \text{ cm}$$

$$W = 1.4 \text{ cm}$$

Fig. 2 - Physical Model and Coordinate System for InSb Cases

to the lack of data on concentration dependency of surface tension and on concentration gradients expected at the free interface.

As with thermogravitational convection, thermocapillary flow will be lamina: with small surface tension driving forces, oscillatory at moderate driving forces and turbulent at large driving forces. The ratio of capillary driving force to resisting viscous force is expressed by the Marangoni number defined as,

$$Ma_L = - \frac{\frac{d\sigma}{dT} \Delta T L}{\rho \nu \alpha}$$

for temperature gradients parallel to the liquid-fluid interface and as

$$Ma_w = - \frac{\frac{d\sigma}{dT} \Delta T W}{\rho \nu \alpha}$$

for temperature gradients perpendicular to the liquid-fluid interface. The symbol σ represents the surface tension and $d\sigma/dT = 0.08 \text{ dyn/cm}^\circ\text{C}$ for InSb (Ref. 5).

A critical Marangoni number has been established for Ma_w (Ref. 6), but not for Ma_L . The dominant temperature gradient for the InSb experiments are parallel to the free surface, thus only values of Ma_L are shown in Table 1.

Table 1
THERMOCAPILLARY CONVECTION SENSITIVITY

Experiment	Liquid	$\frac{\Delta T}{\Delta L} \left(\frac{^\circ\text{C}}{\text{cm}} \right)$	L(cm)	$\frac{d\sigma}{dT} \left(\frac{\text{dyn}}{\text{cm}^\circ\text{C}} \right)$	Ma_L
M560	InSb	15	2 cm	-0.08	35600
M562	InSb	15	6 cm	-0.08	3950
M559	Ge	15	6 cm	-0.60	169000

Even though no firm critical Ma_L is known, values of $Ma_L \geq 7$ exhibited oscillatory laminar flow and $Ma_L \geq 140$ indicated turbulent flow for molten silicon (Ref. 4). It is therefore evident from Table 1 that significant thermocapillary flow should occur in the M560, M562 and M559 experiments.

It should be mentioned at this point, however, that little or no data exist on values of $d\sigma/dT$ in the presence of dopants (such as Te in M562 and Ga in M559) or of oxide films (see Section 4). Neither the Marangoni numbers given in Table 1 nor the analysis by Chang and Wilcox (Ref. 4) account for these phenomena. Thick oxide films may completely suppress thermocapillary convection.

2.3 HEAT AND MASS TRANSFER RATES

Convection affects crystal growth from the melt primarily through its influence on (Ref. 7): (1) the amount of dopant or impurity delivered to the vicinity of the solid-liquid interface; i.e., the rate of mass transfer; and (2) the temperature fluctuations caused near the growth interface (heat transfer). A convenient measure of the convective augmentation to heat transfer is the Nusselt number, Nu. It represents the ratio of total heat transfer to conduction heat transfer and is defined as

$$Nu = hL/k$$

where h is an overall coefficient of heat transfer. It is related to thermal driving forces as follows

$$Nu = C_1 Ra^{C_2} + C_3 Ma^{C_4}$$

where the coefficients C_i are constants.

The constants, C_1 , sometimes incorporate the effects of geometry via the aspect ratio, γ , and the effects of relative diffusivity via the Prandtl number, Pr. The Prandtl number is the ratio of momentum diffusivity ν to thermal diffusivity α . For solutal convection, the Schmidt number, Sc, rather

than Pr is important. The Schmidt number is the ratio of momentum diffusivity to molecular diffusion ($Sc = \nu/D$). Values of Pr and Sc are given later in Table 2.

Transport by convection tends to dominate as Pr or Sc becomes large. These two parameters are also important when estimating mass transfer rates from measured heat transfer rates and vice versa (Ref. 8). The degree of convective augmentation to mass transport is reflected by the Sherwood number, Sh, which is analogous to Nu. For small flow rates, the Sherwood, Nusselt, Schmidt, and Prandtl numbers are related as follows

$$\frac{Sh}{Nu} = \left(\frac{Sc}{Pr} \right)^n \quad (2.1)$$

where $n \approx 1/2$ for laminar flow and $n \approx 1/3$ for turbulent flow. The analogy between heat and mass transfer as embodied by Eq. (2.1), will be utilized in Section 3. There it will be used to estimate mass transfer rates from computed heat transfer rates.

2.4 CONCLUSIONS

Sensitivity calculations indicate that thermogravitational convection will be dominant in ground processing but will not be significant during Skylab processing. Thermocapillary flow should be significant for Skylab in the melt growth experiments with turbulent convection even possible for experiments M562 (InSb) and M559 (Ge). Also the utility of the heat-mass transfer analogy was introduced.

Section 3 COMPUTER PROGRAM MODELS

This section describes the convection analysis, performed via computer program models, of the Skylab experiments M556, M560 and M562. A brief introduction is given to the Lockheed Convection Analysis Program (LOCAP) which was used in the study. A discussion follows which outlines the rationale and assumptions made in formulating mathematical models of these experiments. Results of the computer analysis are then presented in summary tables and in flowfield contour maps. The results consists of heat transfer parameters, velocity magnitudes, flow directions and strengths and temperature profiles in the fluid. A summary of the conclusions reached from the computer analysis itself is given at the end of the section.

3.1 LOCKHEED CONVECTION ANALYSIS PROGRAM (LOCAP)

The quantitative convection analysis of the Skylab experiments was performed using the LOCAP computer solution to the Navier-Stokes equations. LOCAP is a general purpose digital computer code for natural convection analysis. Among the capabilities of the program are: (1) rectangular or cylindrical geometries; (2) gases or liquids; (3) transient and steady-state analysis; (4) confined fluids or free surface flows; (5) time varying body force; (6) temperature-dependent material properties; (7) heating from the side or below; (8) combinations of heat flux and fixed-temperature boundary conditions; and (9) two-dimensional or axisymmetric laminar flow.

A complete formulation of the various models utilized by the program is given in Refs. 9 through 12. A typical formulation using a rectangular geometry is described in Appendix A.

3.2 METHODOLOGY OF COMPUTER MODELS

A mathematical model of a physical system must contain the important parameters and constraints of the physical problem and yet be simple enough to allow solutions to be obtained. The approach taken in this analysis is to make assumptions which allow the experiments to be modeled using LOCAP, and yet still retain the governing parameters of the real experimental configuration. These assumptions are outlined below:

- The flow is assumed to be two-dimensional.
- Containers of rectangular cross section are used. This was necessary in some cases to avoid three-dimensional situations which occur in cylindrical geometries.
- Only the liquid phase of the experiment is modeled. Freezing/melting processes, latent heat effects and moving solid boundaries are not considered.
- Boundaries of two types are considered: (1) rigid, solid wall boundaries, and (2) free liquid surface boundaries, i.e., liquid-vapor interface.
- Accelerations (body forces) are in one direction only; either parallel to or perpendicular to the heating direction. The mean g-level is taken to be $2.0 \times 10^{-4} g_E$. "G-jitter" is also considered.
- Heat is supplied to the fluid through constant temperature boundary conditions.
- All material properties, except density, are assumed to be constant. Table 2 gives the values used in the computer models.

Some of the above assumptions may appear to be severe, however, after careful examination, we found that (1) this type of model will provide quantitative information to the experiment Principal Investigator, and (2) the current state of the art does not permit any solutions at all for three-dimensional convection with a melting/freezing interface and free liquid surfaces.

Table 2

MATERIAL PROPERTIES USED IN COMPUTER MODELS

Property Material	Thermal Conductivity $\frac{\text{cal}}{\text{cm}\cdot\text{sec}\cdot^{\circ}\text{C}}$	Dynamic Viscosity (poise)	Density (gm/cm^3)	Specific Heat ($\text{cal}/\text{gm}\cdot^{\circ}\text{C}$)	Thermal Expansion Coefficient ($1/^{\circ}\text{C}$)	Prandtl Number (ν/α)	Schmidt Number*, (ν/D)
Ge I ₄	$9.44 \cdot 10^{-6}$	$2.30 \cdot 10^{-4}$	$1.456 \cdot 10^{-2}$	$4.46 \cdot 10^{-2}$	$7.55 \cdot 10^{-4}$	1.086	1.5
In Sb	$8.00 \cdot 10^{-2}$	$1.20 \cdot 10^{-2}$	6.8	$6.54 \cdot 10^{-2}$	$1.00 \cdot 10^{-4}$	$9.8 \cdot 10^{-3}$	4
Ge	$4.30 \cdot 10^{-2}$	$7.50 \cdot 10^{-3}$	5.6	$9.00 \cdot 10^{-2}$	$1.00 \cdot 10^{-4}$	$1.57 \cdot 10^{-2}$	10
Water (for com- parison) 38°C	$1.50 \cdot 10^{-3}$	$6.82 \cdot 10^{-3}$	0.992	0.998	$3.60 \cdot 10^{-4}$	4.52	1000

* Taken from Ref. 4 or estimated using Refs. 13 and 14.

The configuration and governing parameters for the Ge I_4 model were shown in Fig. 1. The Ge I_4 gas is contained by rigid walls with rectangular cross section 15 cm x 1.4 cm. Figure 2 displays the corresponding configuration for the InSb experiment model. The rectangular container is 6.0 cm x 1.4 cm and the liquid InSb may be totally confined or have one or two free surfaces at the upper and lower long walls. The matrix of cases run on the computer for each of these two experiments is given in the next subsection in which the results of the models is discussed. The final case considered uses the Fig. 2 geometry with germanium replacing the InSb as the liquid melt.

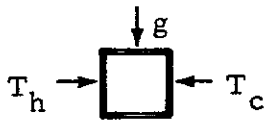
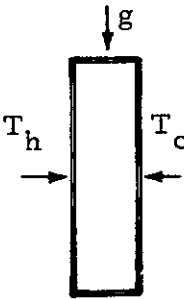

3.3 Ge I_4 MODEL RESULTS

Table 3 summarizes the results of the Ge I_4 computer models. Three aspect ratios were considered as shown with Case G3 being the configuration which most closely models the M556 experiment. Case G1 was processed to: (1) checkout the program for Ge I_4 gas; (2) provide a comparison of aspect ratio effects; and (3) provide a starting solution for the larger aspect ratio cases. Case G2 was run for similar reasons. As Table 3 shows, the influence of buoyancy driven convection on this experiment is small.

The largest velocity calculated is 0.0025 cm/sec which does not appreciably affect the heat transfer ($\text{Nu} \approx 1$). Similarly for $\text{Sc} \approx 1.5$, the mass transfer for growing the crystal is not appreciably affected by these small velocities ($\text{Sh} \approx 1$). It is interesting to note that Case G3 produces the smallest flow velocities of any of the three cases studied.

In addition to these "constant g" cases, the influence of time-varying accelerations or g-jitter were studied. Models of the g-jitter using sine wave, cosine wave, and "sawtooth" profiles with a range of amplitudes and periods were tested. Amplitudes of even 10^{-3} g at periods of 0.1 sec to 10 sec showed no appreciable change from the comparable constant-g case. We conclude that most of the realistic jitter that could have been present on Skylab would not have a detectable influence on the M556 experiment.

Table 3
 SUMMARY OF GeI_4 CALCULATIONS
 ($g = 2 \cdot 10^{-4} g_E$)

Case No.	Grashoff Number Based on Vertical Dimension	Aspect Ratio, H/L	Configuration and Orientation	Maximum Velocity (cm/sec)	Nusselt No.	Sherwood No.
G1	1.1×10^4	1.0		0.072	1.008	1.18
G2	2.0×10^5	10.71		0.014	1.004	1.17
G3	1.6×10^2	0.093		0.0025	1.000	1.16

Details of the flow patterns and temperature distributions for each of these cases are shown in Figs. 3, 4 and 5. The velocity vector plots are shown in the x-y plane with the arrow indicating direction of the flow and the length of the line denoting relative magnitude. The isotherm maps are lines of constant temperature plotted in the x-y plane. The isotherms which are not straight indicate some influence of the flow on the heat transfer.

Figure 3 is for Case G1 in which the flow is seen to be a single cell somewhat near the bottom of the container. The boundary layer at the left and right walls appear to be well resolved in this solution. The isotherm maps are not perfectly straight indicating some (small) influence of the flow on the heat transfer.

Figure 4 is for Case G2 where the flow is seen to consist of one long cell going up the hot wall, down the cooler wall and nearly centered in the container. The isotherm maps are straight except near the extreme ends where the heat transfer is affected the greatest.

Case G3 is shown in Fig. 5. Note that the isotherms are almost perfectly straight indicating a conduction-dominated situation. The streamline maps are shown here in addition to the velocity vector maps to better identify the flow pattern. These plots were generated at 800 sec after heating began. The streamlines show that a two-cell unsteady pattern still exists with a one-cell pattern around them. This is apparently a remnant of the unsteady part of the calculation and the flow should develop into a single long cell at steady state. The solution was stopped after 800 sec due to long computer run times. The results were then extrapolated to quasi-steady state.

The results of the Ge I₄ computer models have shown that flow can be induced at $g = 2 \times 10^{-4}$ but is relatively weak. The heat transfer is affected very little by this flow, as is mass transfer.

↓
 $g = 2 \times 10^{-4} g_E$

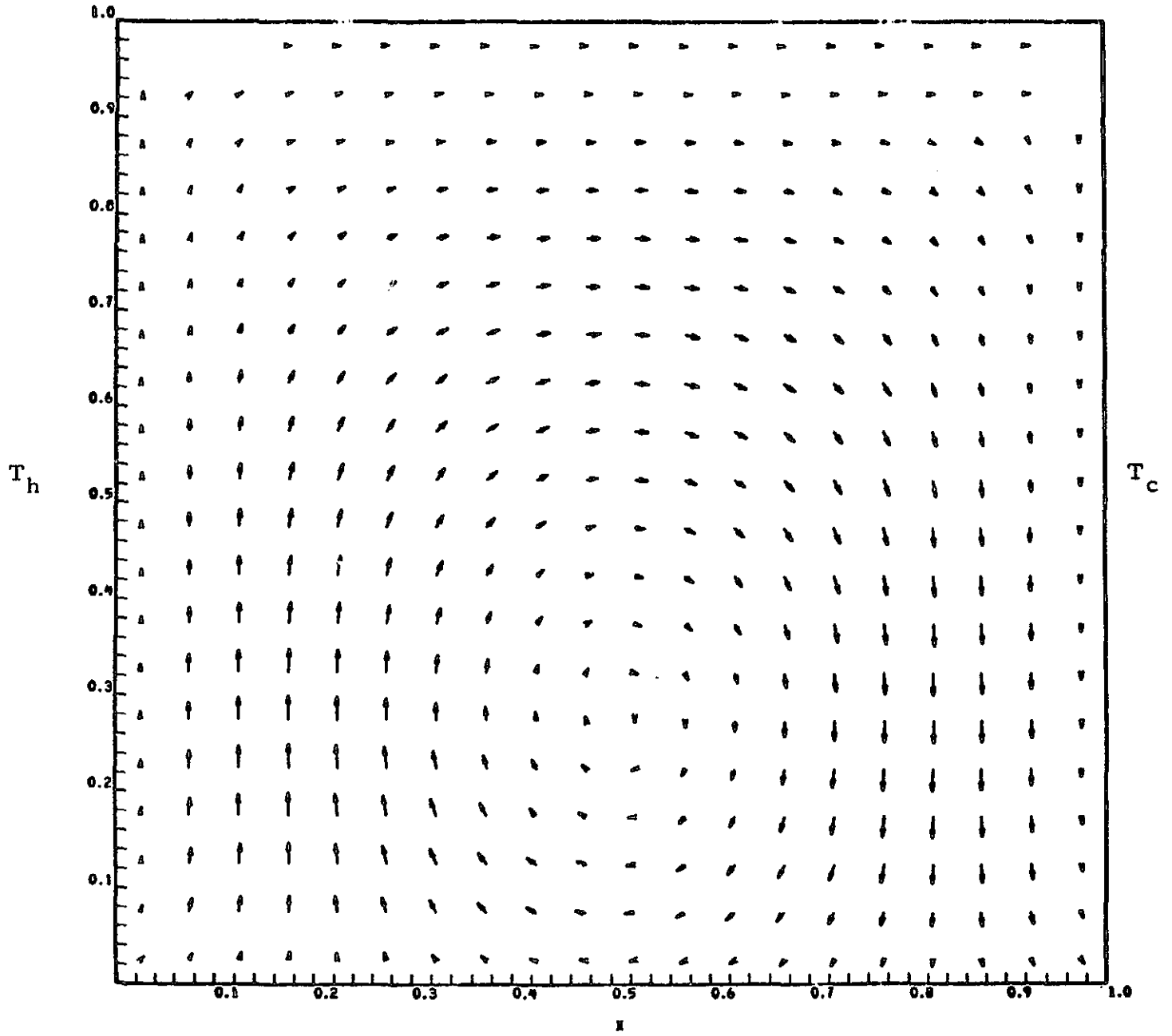


Fig. 3a - Velocity Vector Map for $Ge I_4$ (Case G1), Aspect Ratio $\eta = 1$

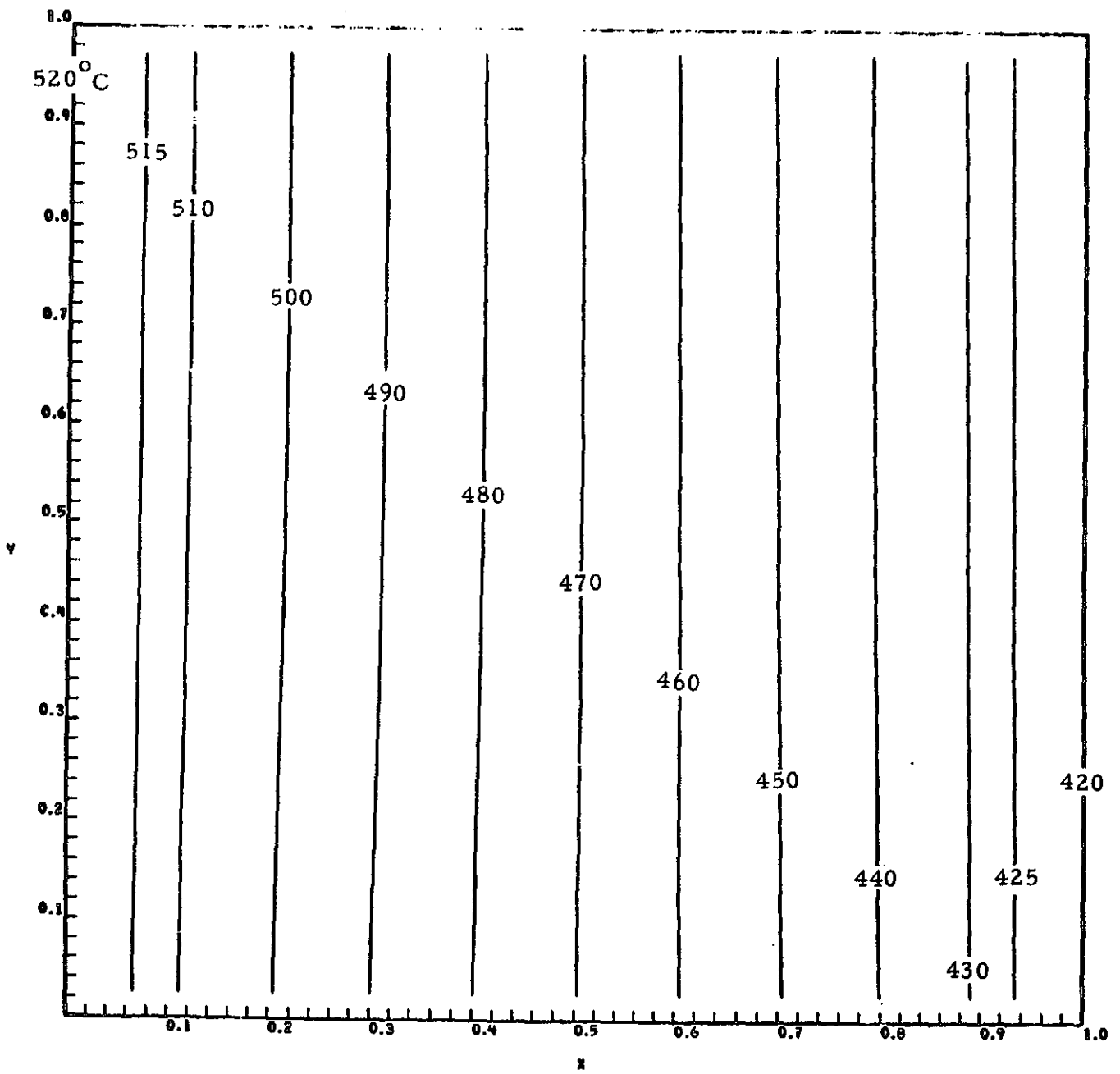


Fig. 3b - Isotherm Map for GeI₄ (Case G1), Aspect Ratio η = 1

↓
 $g = 2 \times 10^{-4} g_E$

Short Wall

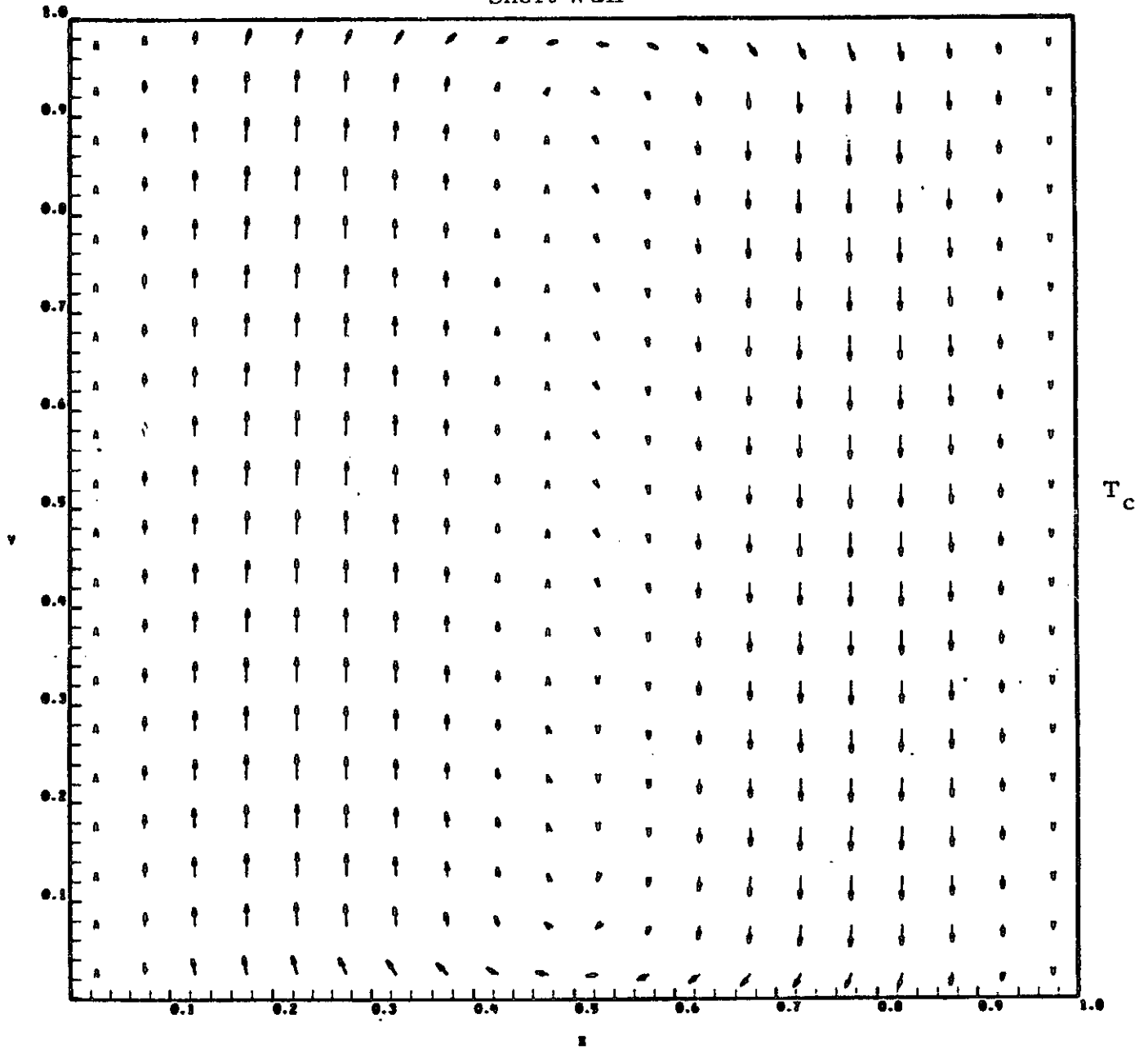


Fig.4a - Velocity Vector Map for Ge L_2 (Case G2), Aspect Ratio $\eta = 10.71$

↓ $g = 2 \times 10^{-4} g_E$

Short Wall

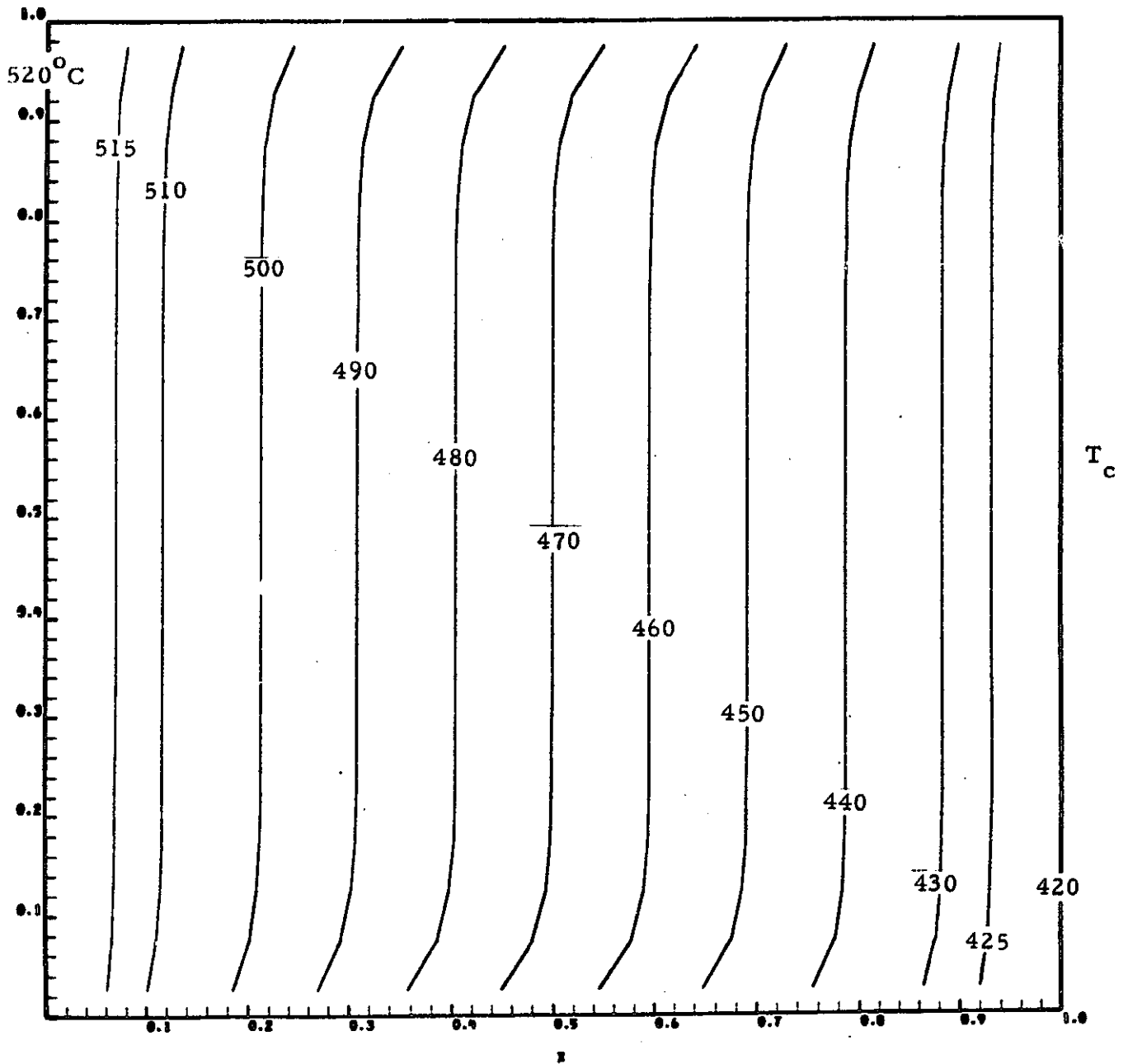


Fig. 4b - Isotherm Map for GeI_4 (Case G2), Aspect Ratio $\eta = 10.71$

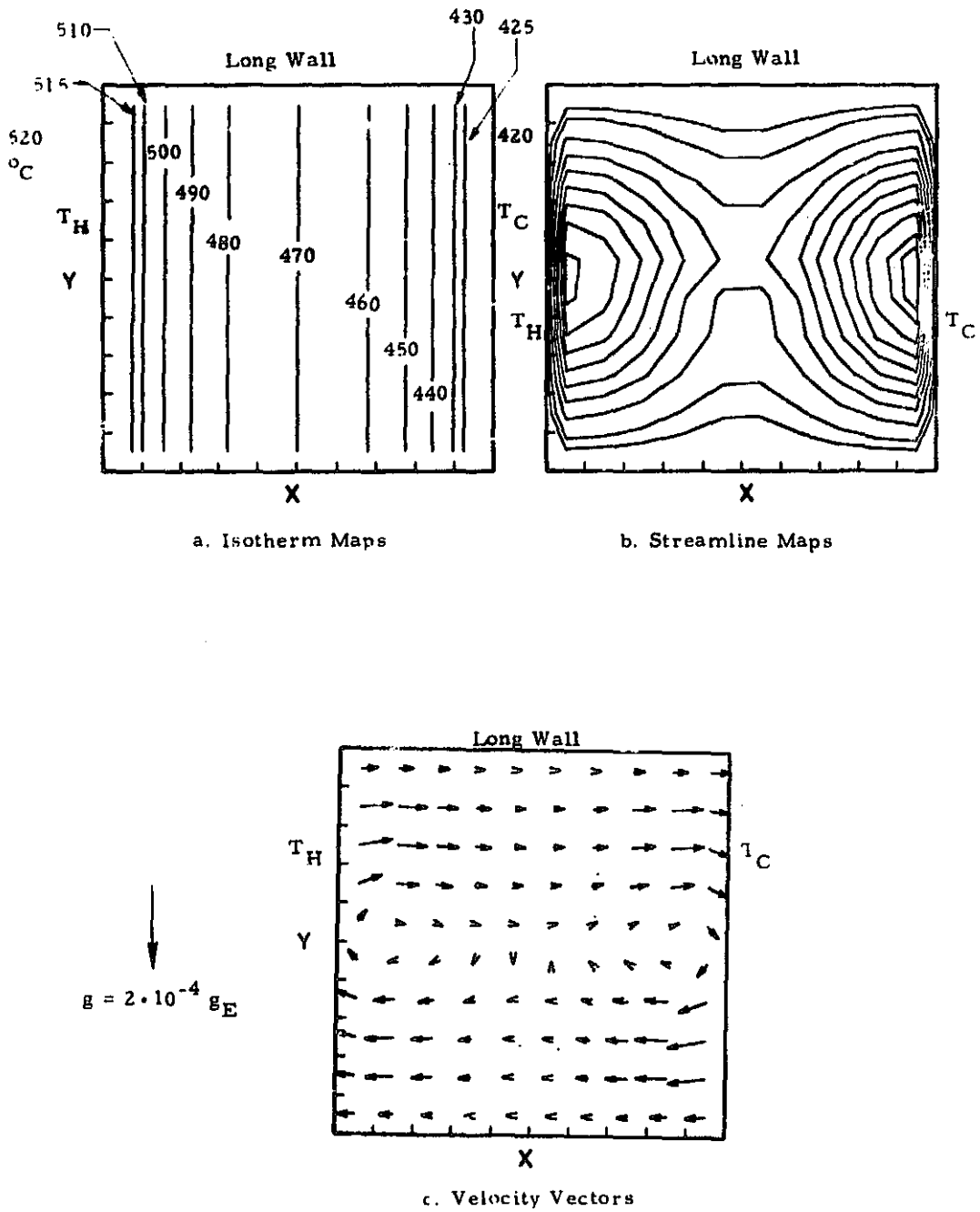


Fig. 5 - Isotherm, Streamline and Velocity Vector Maps for Ge I₄ (case G3); Aspect Ratio = 0.093 (at t = 800 sec).

3.4 InSb MODEL RESULTS

Table 4 summarizes the results of the calculations for the InSb cases. Case 11 consists of a confined region of InSb (no free surfaces) so that only buoyancy-driven convection is possible. Cases 12, 13, 14 consist of both buoyancy effects and surface tension driven from on the "top" surface only. Cases 15 through 18 are for $g = 0$ with free surfaces along both long walls.

A range of values of the surface tension gradient with temperature was used due to uncertainty in the data for this parameter. The free surface boundary condition is derived by equating the shear stress to the surface tension gradient. This provides an expression for the velocity gradient at the surface in terms of the Prandtl number and Marangoni number.

Table 4 shows a range of Marangoni numbers from 11.7 to 11,700. The highest value corresponds to $\partial\sigma/\partial T = -0.07$ dyne/cm- $^{\circ}$ C which is the upper limit of the data found in the literature (Ref. 5). The table shows that buoyancy convection produces velocities ~ 0.011 cm/sec and no detectable influence of the heat transfer ($\overline{Nu} = 1.000$). However, the free surface effects appear to be quite drastic. Case 14 corresponds to an order of magnitude less surface tension gradient than the literature data indicates, yet a maximum flow velocity of ~ 0.871 cm/sec is calculated with $\sim 18\%$ increase in heat transfer. The mass transfer induced by this relatively large velocity will be even more severe. In fact, utilization of Eq. (1) indicates $Sh \gg 1$, which should appreciably affect dopant distribution.

Case 18 probably corresponds more closely to the true experiment conditions; two free surfaces with $Ma = 11,700$. The flow velocity calculated is ~ 2.41 cm/sec with a $\sim 67\%$ increase in heat transfer. This case and its implications and comparison to the actual experiment results are given in Section 4.

Table 4
SUMMARY OF InSb CALCULATIONS

Case No.	Gravity Level (g)	Number of Free Surfaces	Marangoni No. (Ma)	Nusselt No. (\bar{Nu})	Maximum Velocity (cm/sec)	Sherwood No. (Sh)
11	2×10^{-4}	0	--	1.000	0.011	
12	2×10^{-4}	1	11.7	1.003	0.071	20.1
13	2×10^{-4}	1	117.	1.026	0.258	20.5
14	2×10^{-4}	1	1170.	1.185	0.871	23.7
15	0.0	2	11.7	1.002	0.065	20.0
16	0.0	2	117.	1.017	0.237	20.3
17	0.0	2	1170.	1.167	0.346	23.3
18	0.0	2	11,700.	1.673	2.41	39.0

Figures 6 through 13 show the details of the calculations for each of the eight cases, respectively. The figures (a) show the velocity vector maps in the x-y plane. The arrow indicates the direction of the flow and the length of the line gives the relative magnitude. The length of the longest line shown corresponds to the maximum velocities of Table 4.

Figure 6 shows that one long cell is induced in the container for the buoyancy driven case. The isotherms are very straight indicating that conduction is the dominant heat transfer mechanism. Comparison of Figs. 6a and 7a shows the influence of a free surface. The flow pattern in Fig. 7a shows that the cell is nearer to the top of the region than the buoyant cell in Fig. 6a.

Figures 8 and 9 show the effects of increasing Marangoni number on the flow profile. A comparison of Figs. 7b, 8b and 9b for the streamlines indicates that the cell center moves closer to the "cool" wall as the Marangoni number is increased. The strength of the flow also increases as shown by the streamline magnitude at the center of the cells. The isotherm maps in Figs. 7c, 8c and 9c give a picture of the influence of the convection on the heat transfer. The isotherms are no longer straight for the larger Marangoni number cases.

Figures 10 through 13 are similar flow maps for the cases having two free surfaces. The velocity vector and streamline maps show the two cell patterns which result from surface tension driven flow on both the long walls. No buoyancy effects are included since Case II showed that thermogravitational convection is negligible. The isotherm maps progress from almost straight lines for $Ma = 11.7$ to very curved patterns for the $Ma = 11,700$ case. The Case I8 is particularly significant since this corresponds more closely to the actual experiment conditions. The calculations give a relatively large velocity, ~ 2.4 cm/sec, induce $\sim 67\%$ increase in the heat transfer, could drastically affect mass transfer and from the shape of the isotherms could produce a non-flat crystal growth interface. Further discussion of this case in conjunction with the actual M560 and M562 experiment findings is given in the next section.

Long Wall

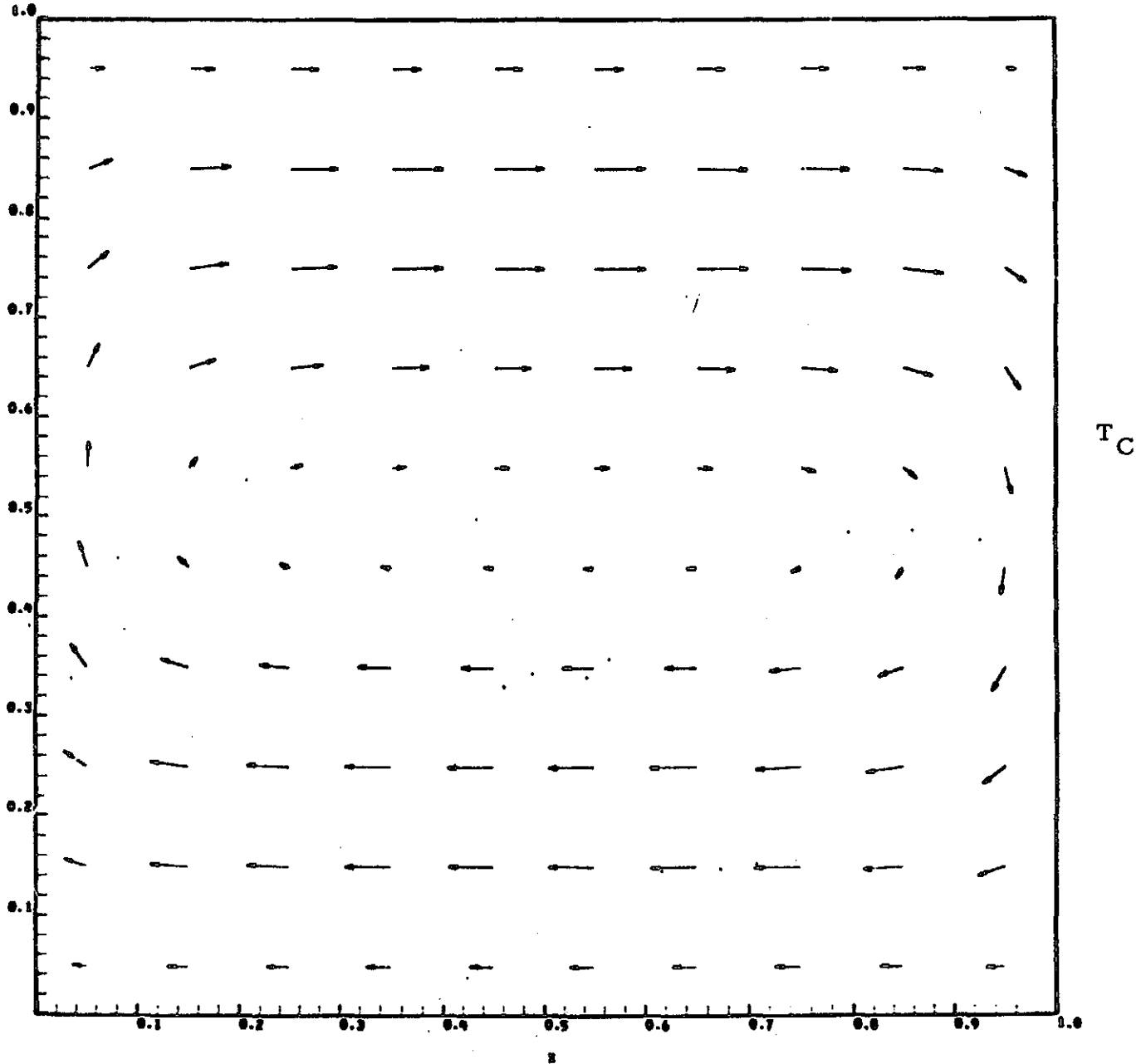
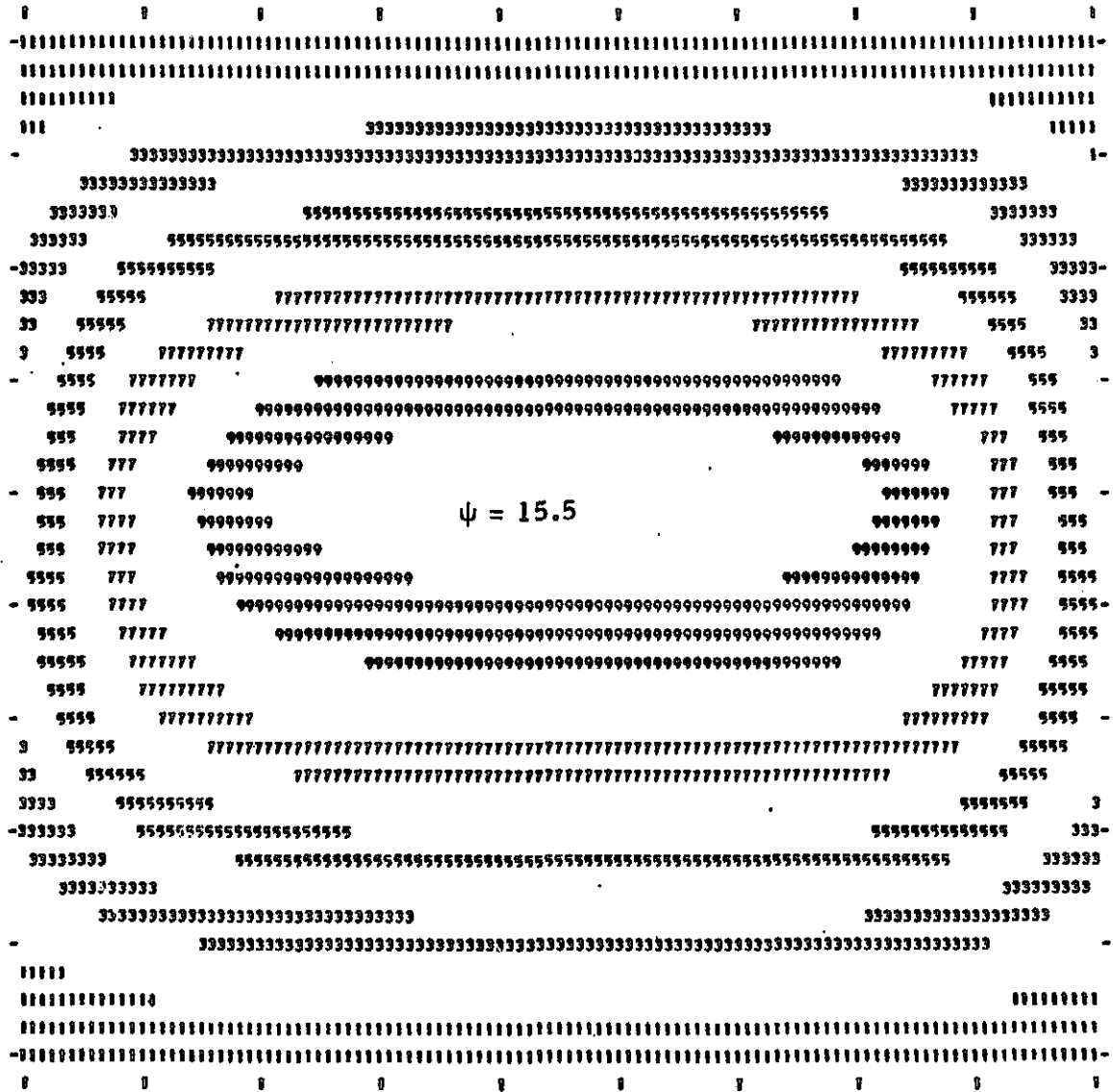


Fig. 6a - Velocity Vector Map for InSb Case 11 (No Free Surface)

Long Wall

.637530+01 .790023+01
 .155725+02



T_H

T_C

Fig. 6b - Streamline Map for InSb Case I1 (No Free Surface)

Long Wall

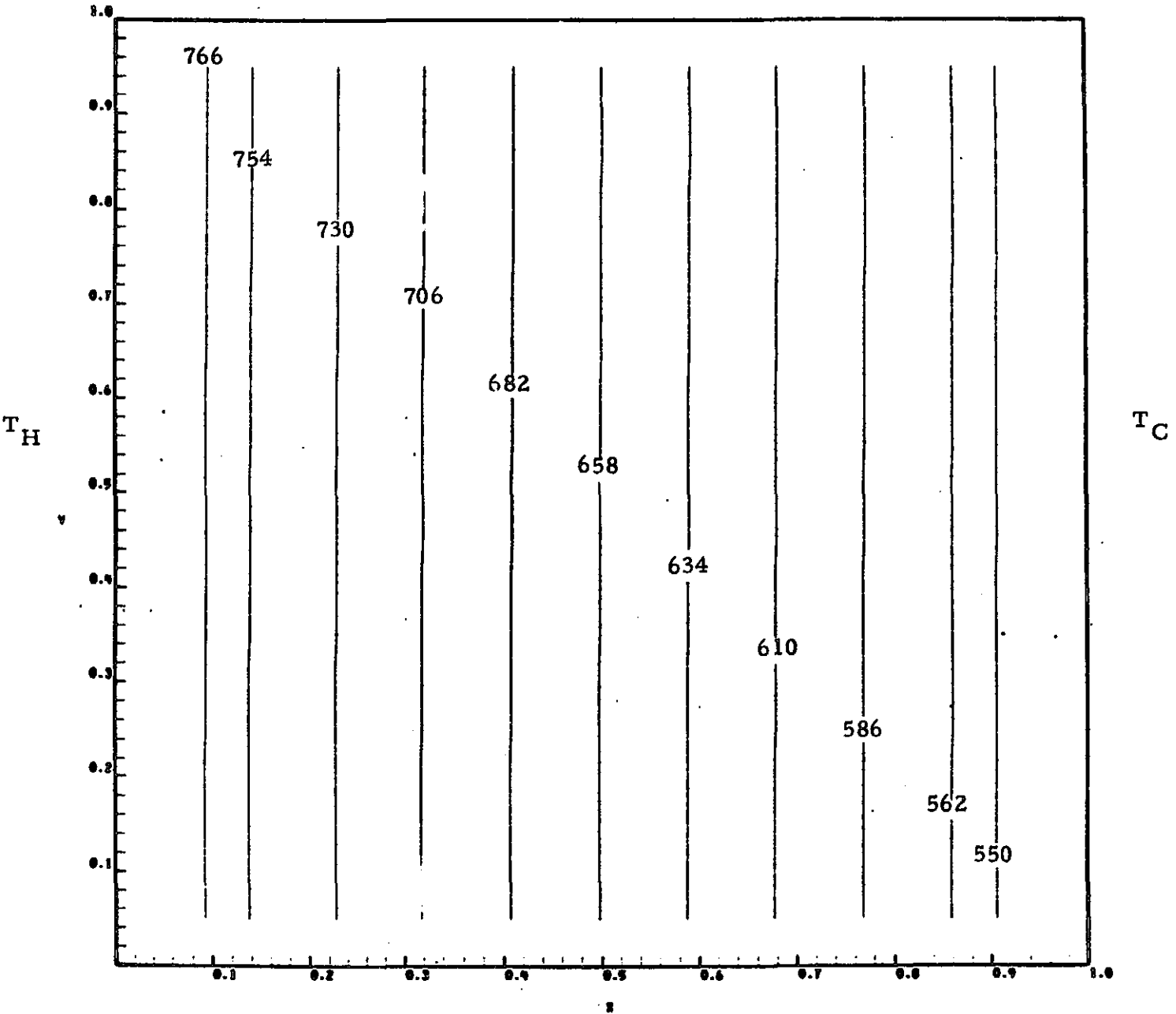


Fig. 6c - Isotherm Maps for InS¹ Case 11 (No Free Surface)

Long Wall

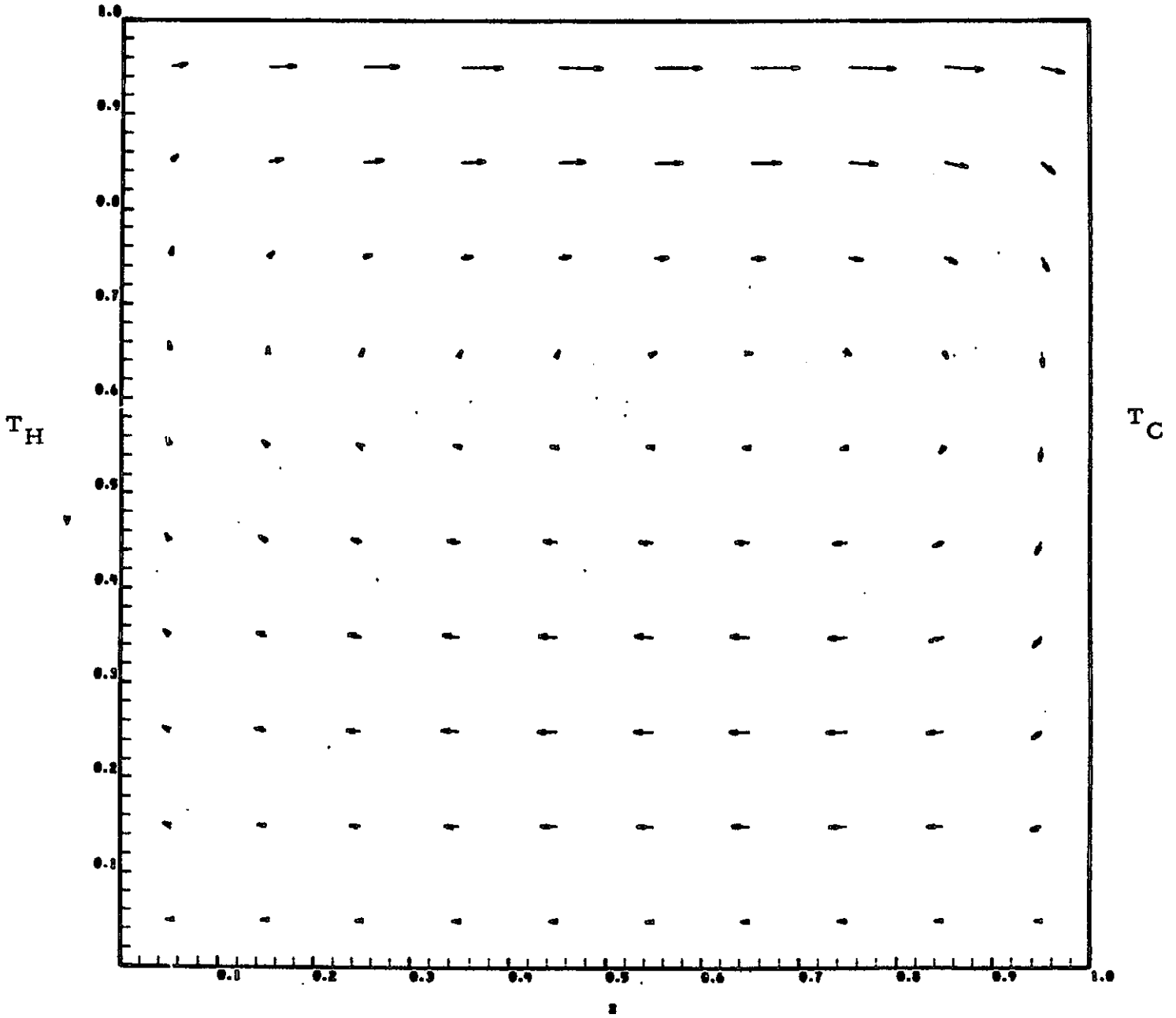


Fig. 7a - Velocity Vector Map in InSb Case 12 (Free Surface Ma = 11.7)

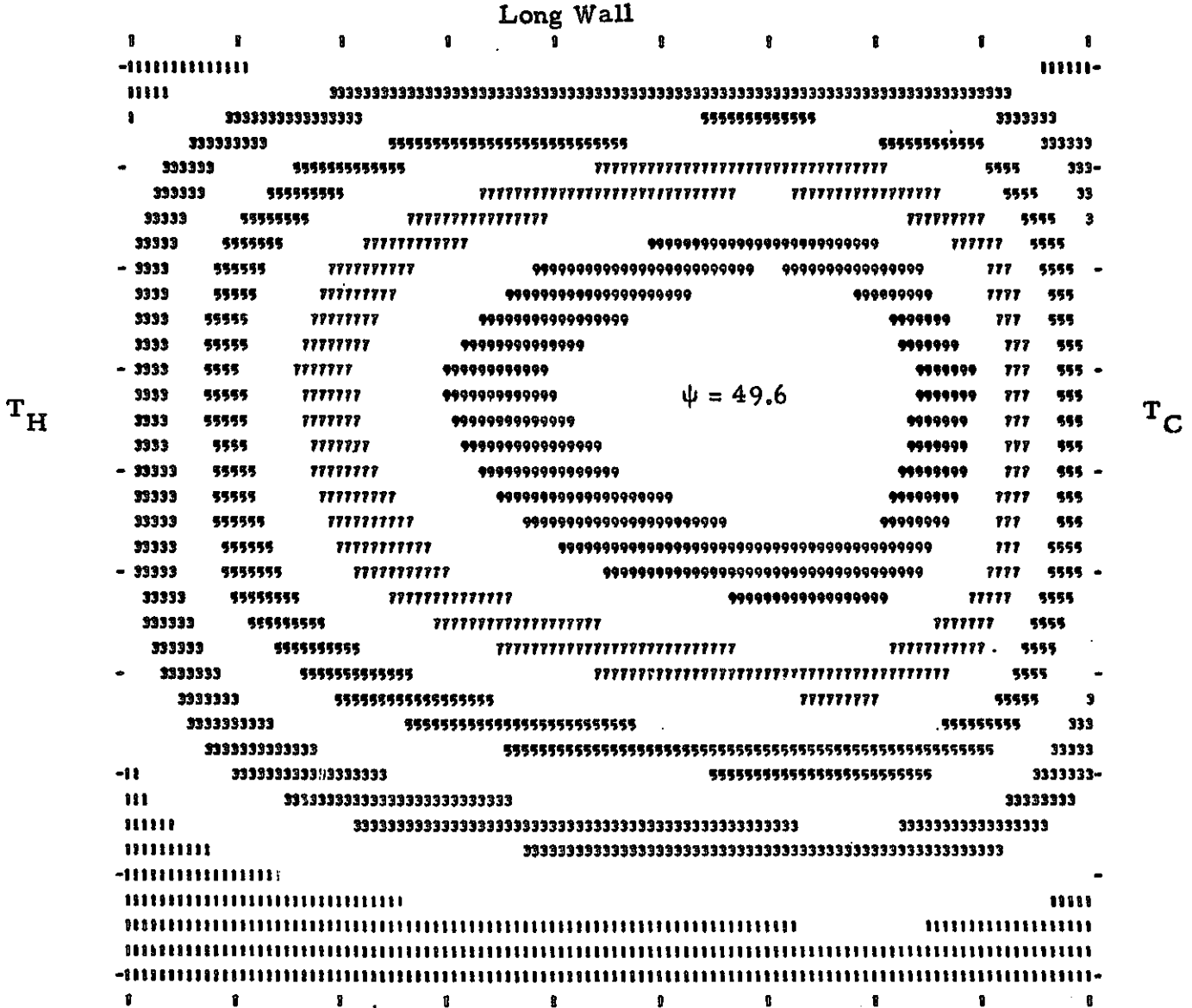


Fig. 7b - Streamline Maps for InSb Case I2 (Free Surface Ma = 11.7)

Long Wall

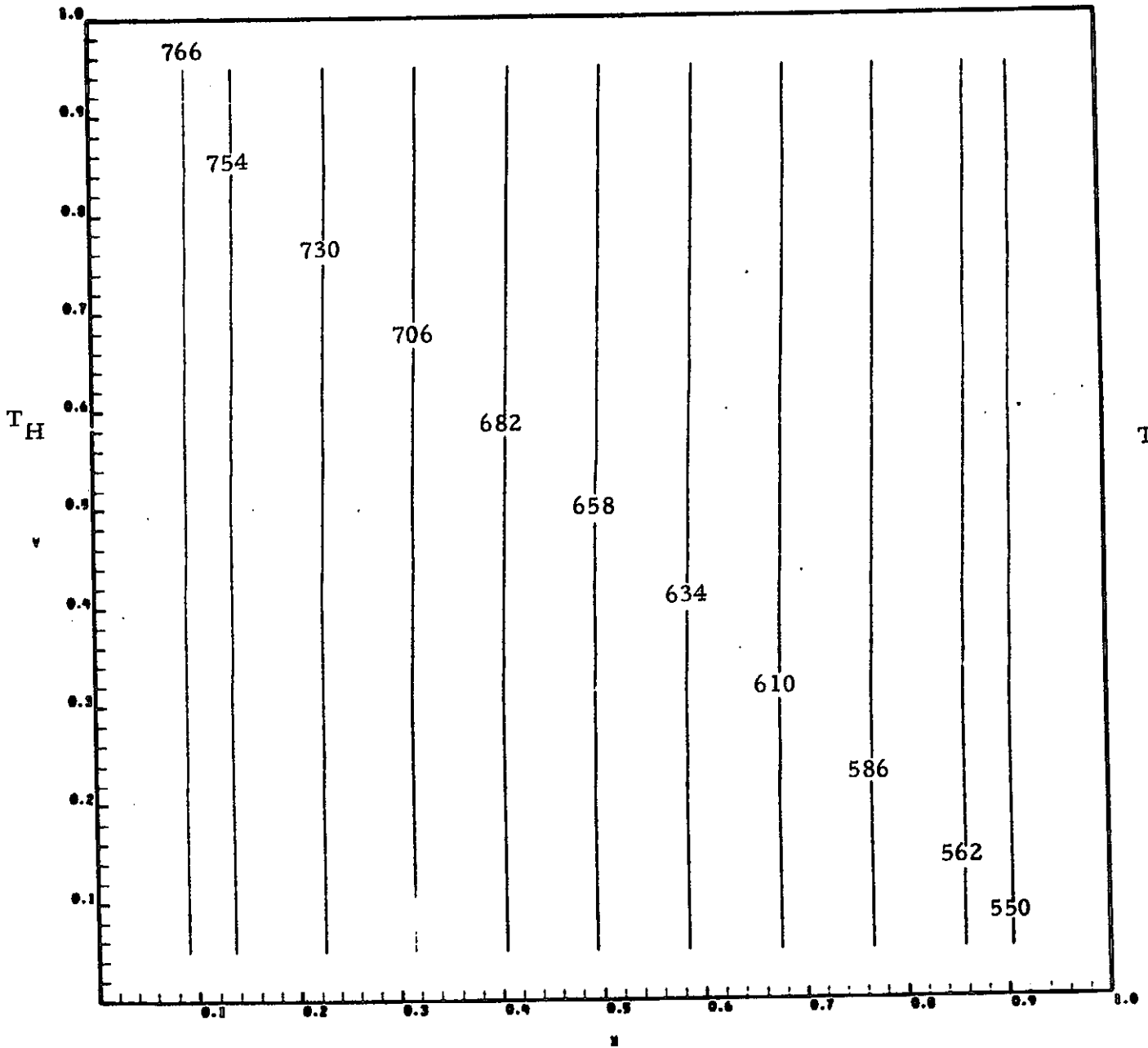


Fig. 7c - Isotherm Map for InSb Case 12 (Free Surface $Ma = 11.7$)

Long Wall

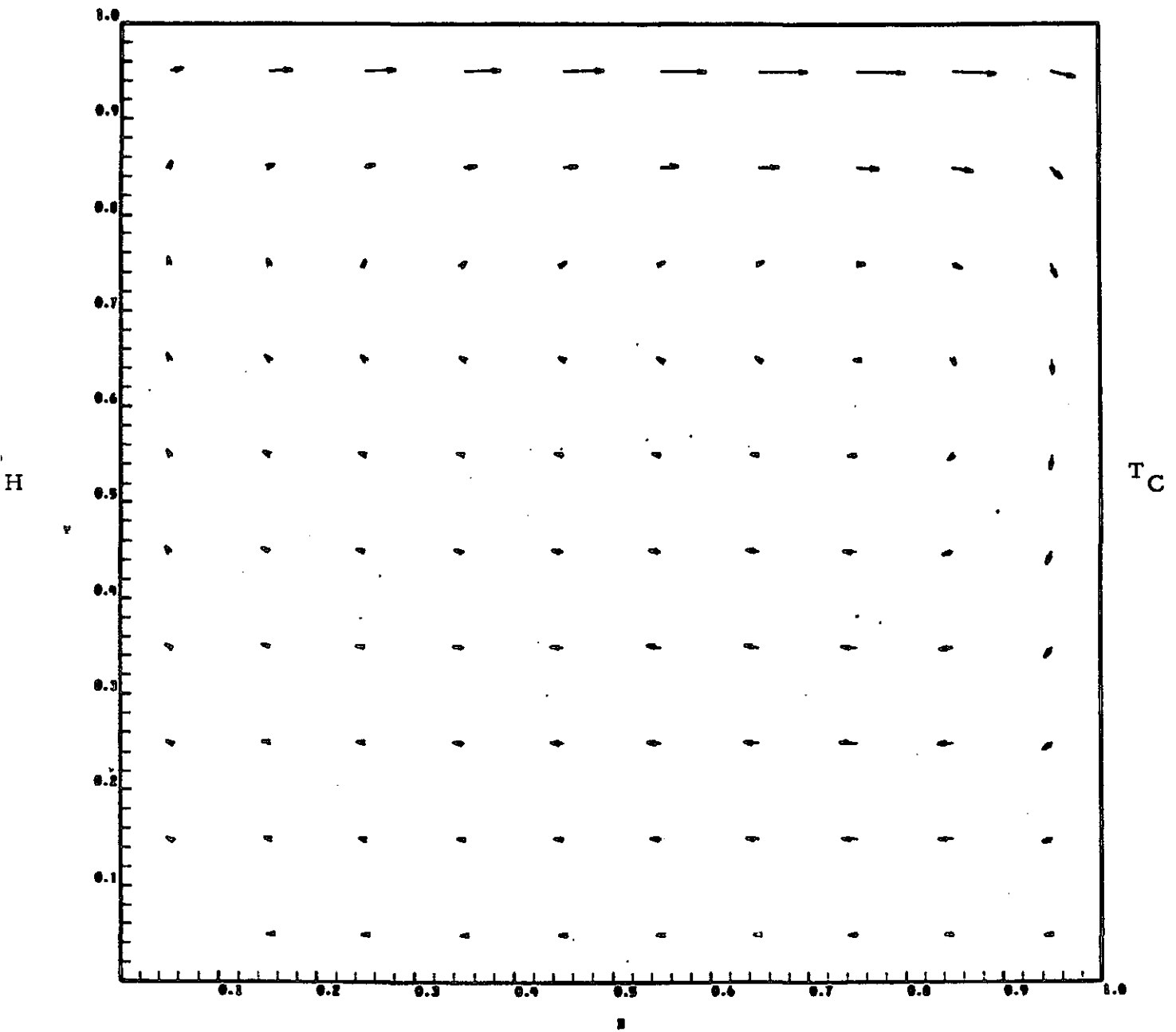


Fig. 8a - Velocity Vector Map for InSb Case 13 (Free Surface Ma = 117)

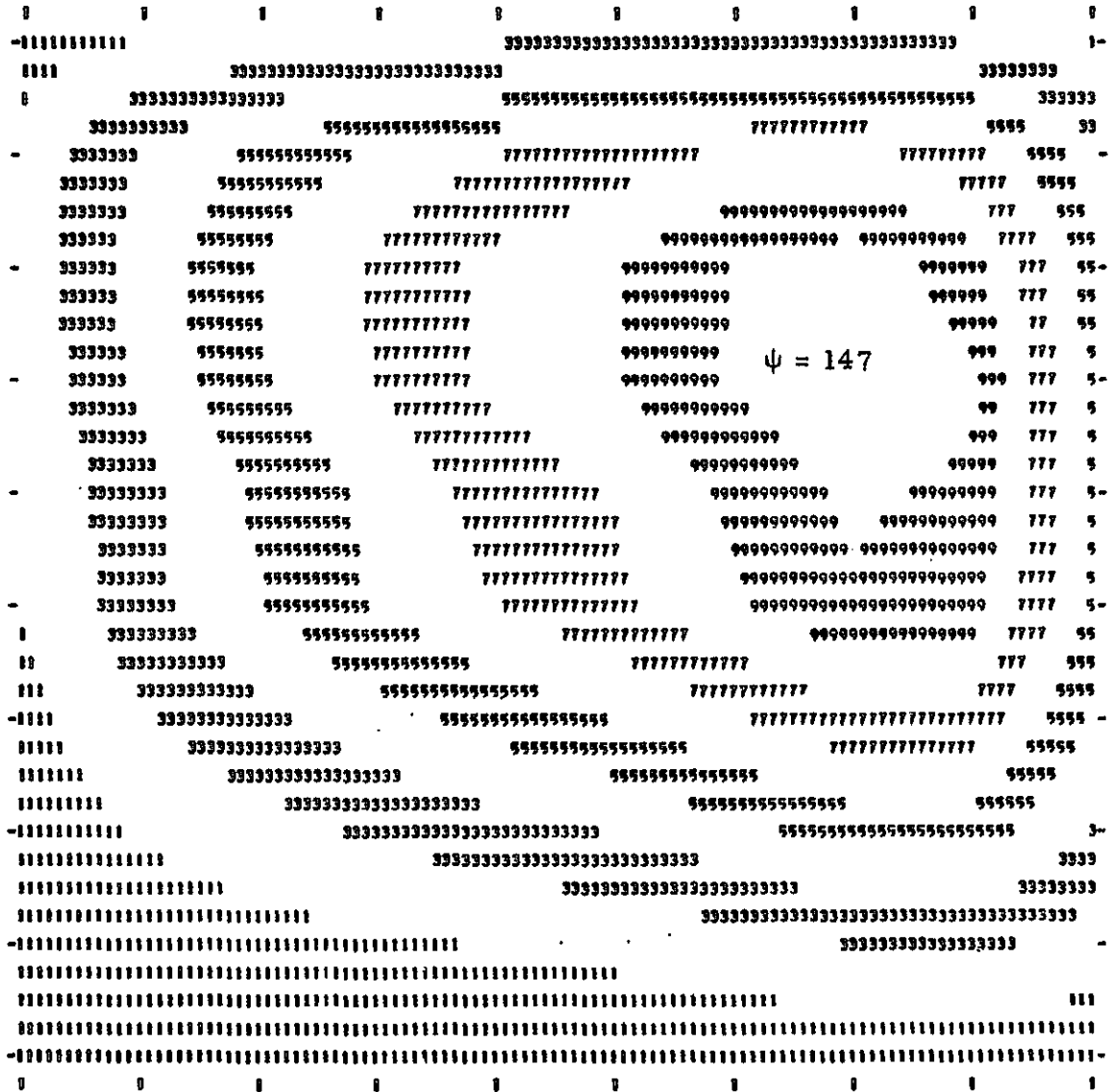


Fig. 8b - Streamline Map for InSb Case I3 (Free Surface Ma = 117)

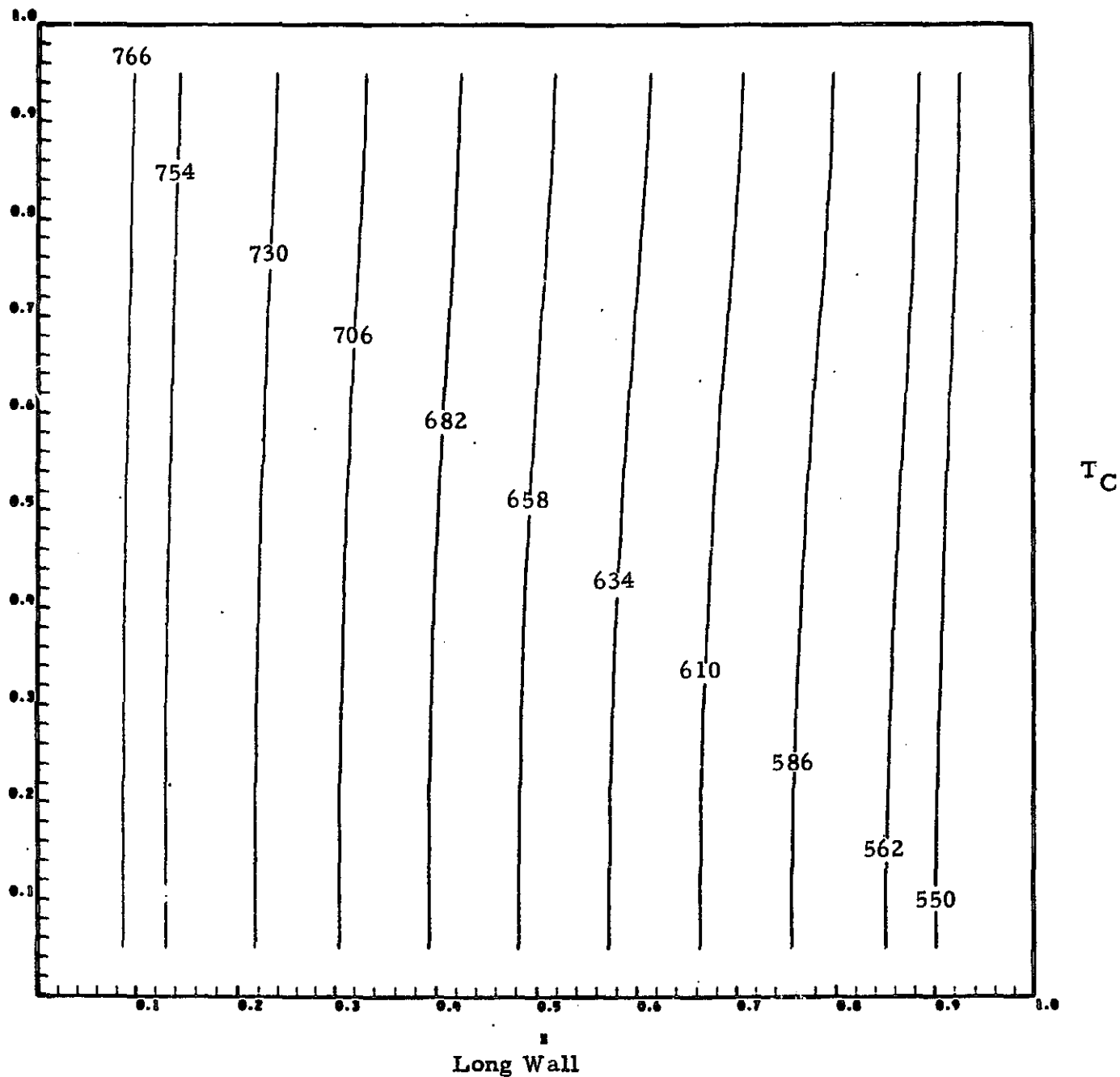


Fig. 8c - Isotherm Maps for InSb Case I3 (Free Surface Ma = 117)

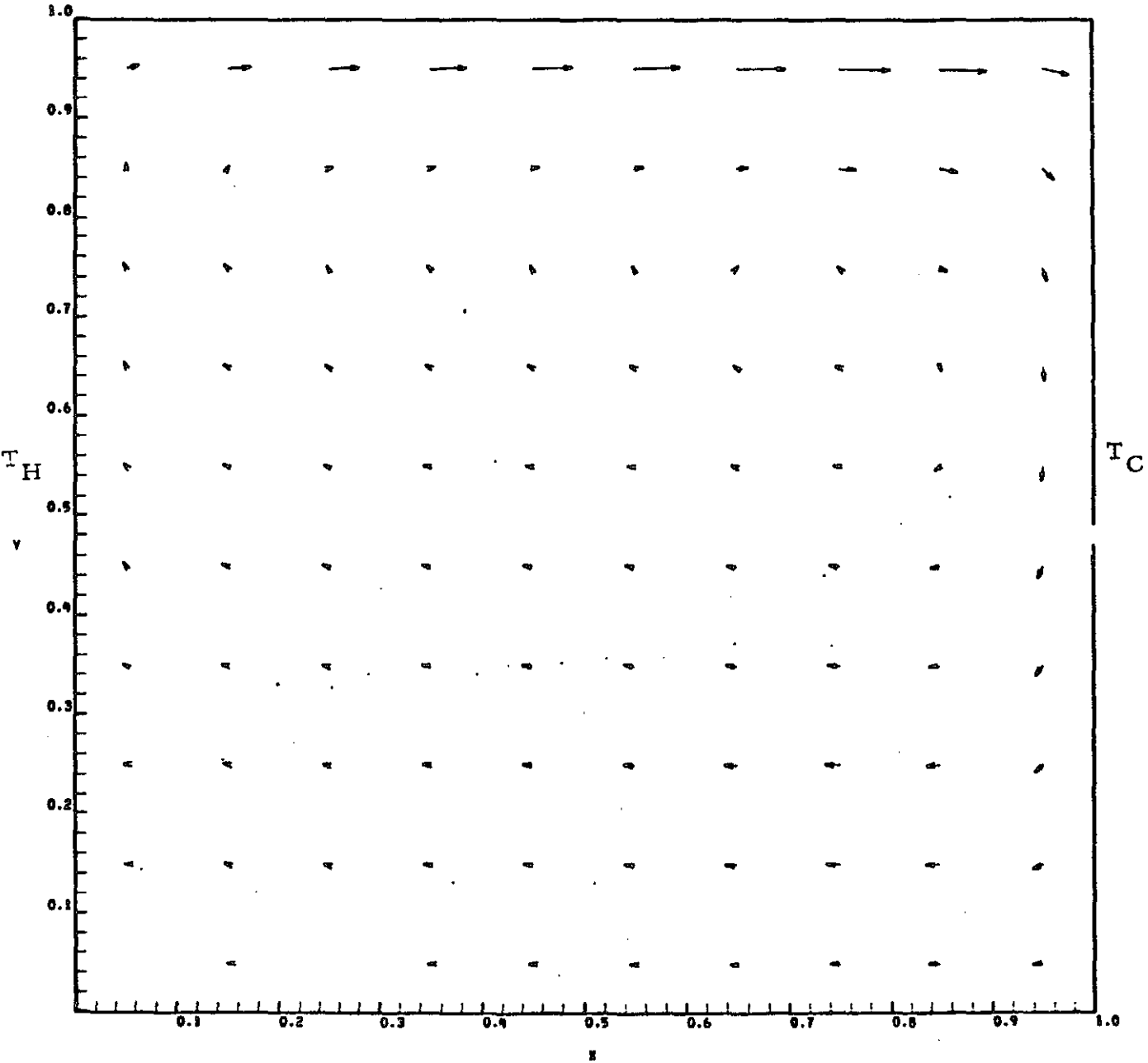


Fig. 9a - Velocity Vector Map for InSb Case I4 (Free Surface, Ma = 1170)

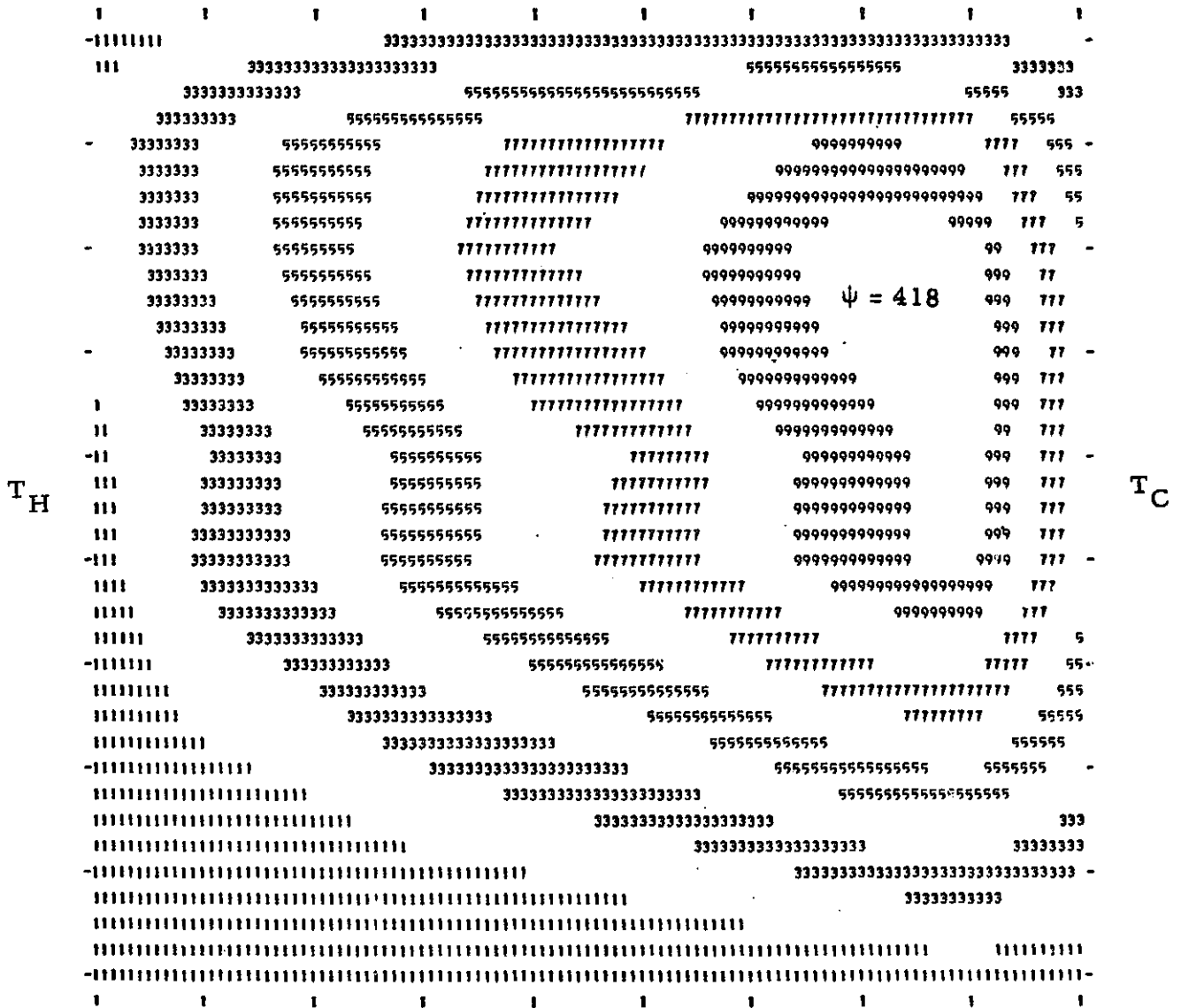


Fig. 9b - Streamline Map for InSb Case I4 (Free Surface, $Ma = 1170$)

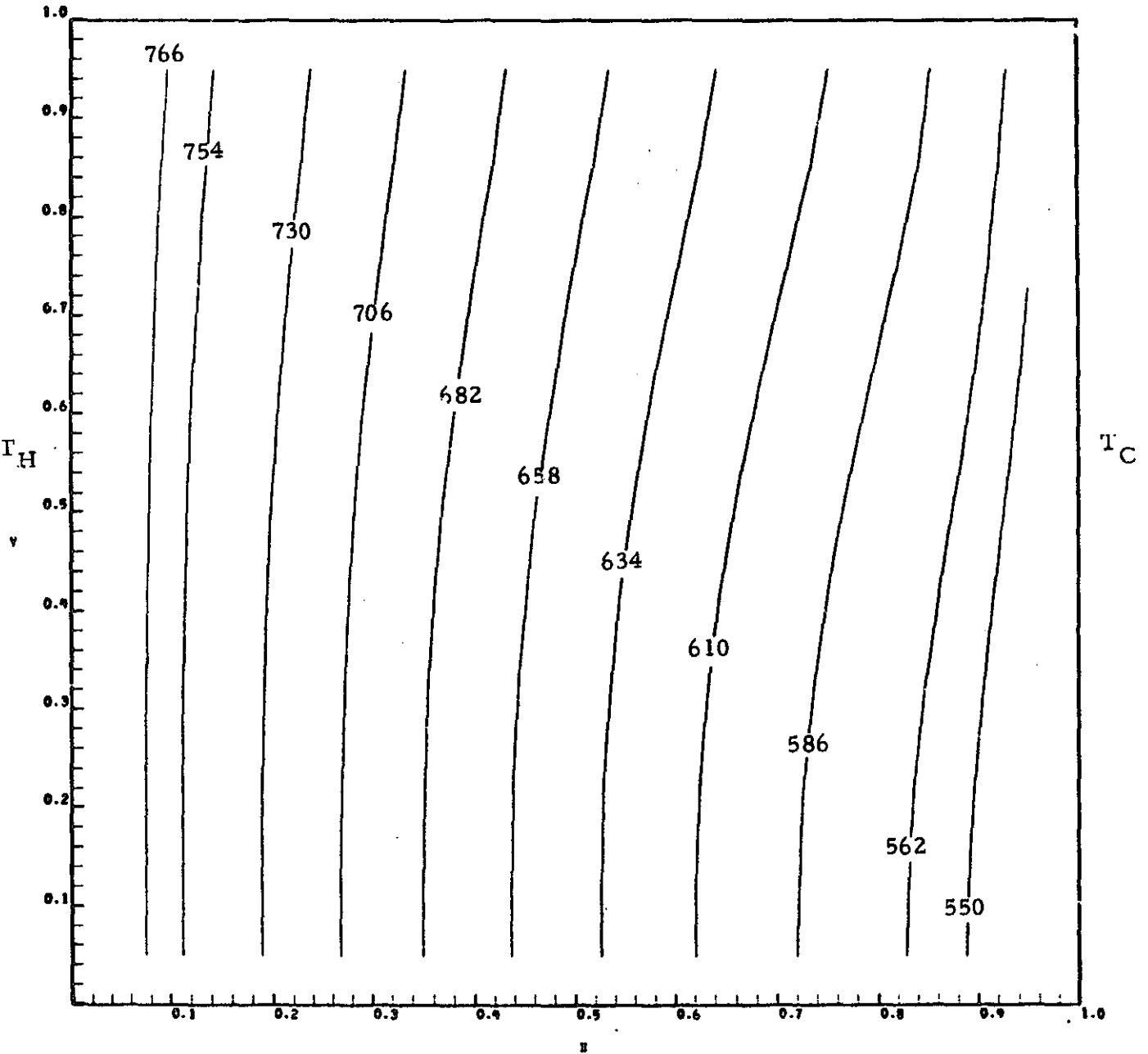


Fig. 9c - Isotherm Map for InSb Case I4 (Free Surface, $Ma = 1170$)

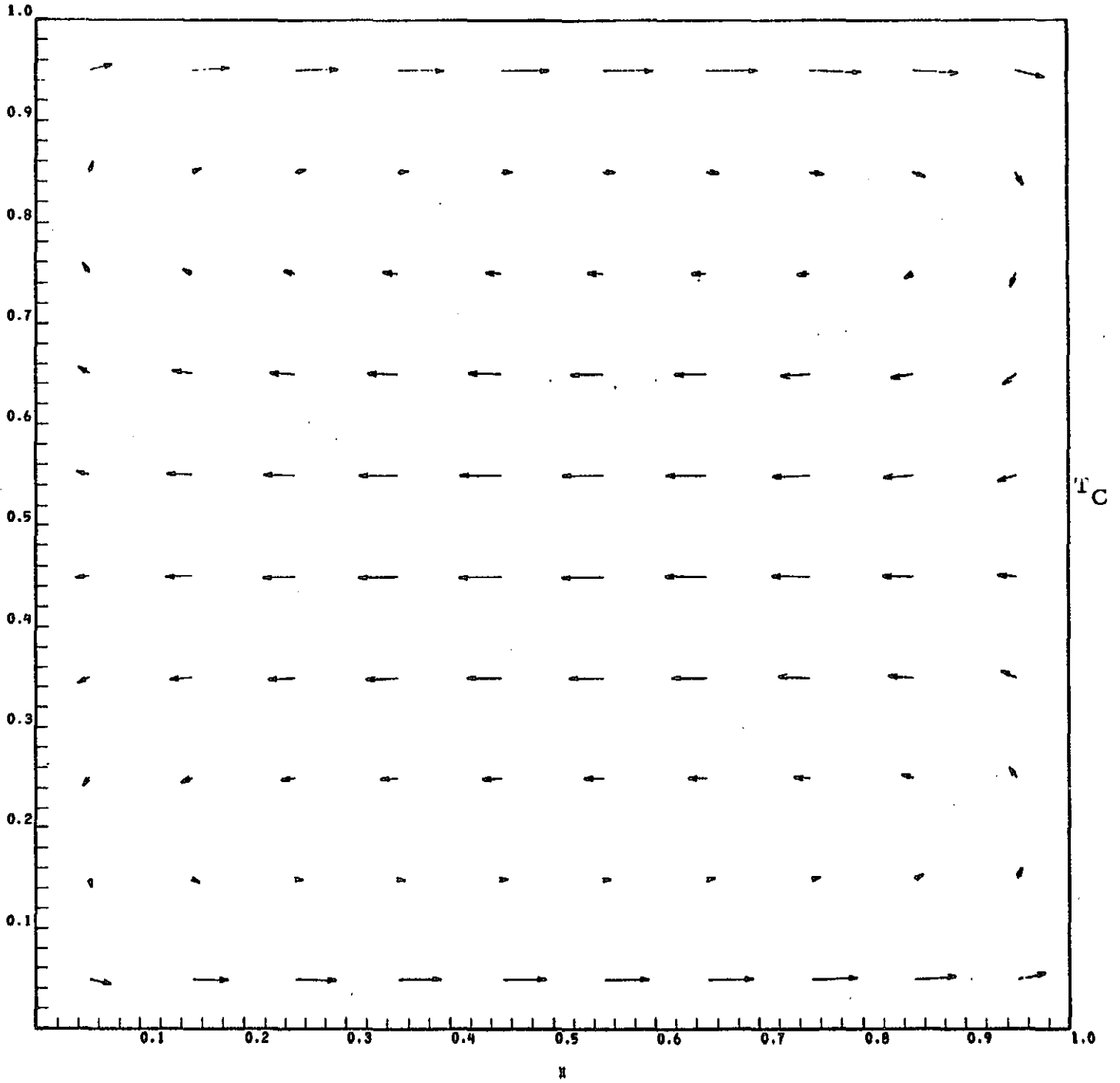


Fig. 10a - Velocity Vector Map for InSb Case 5 (Two Free Surfaces, Ma = 11.7)

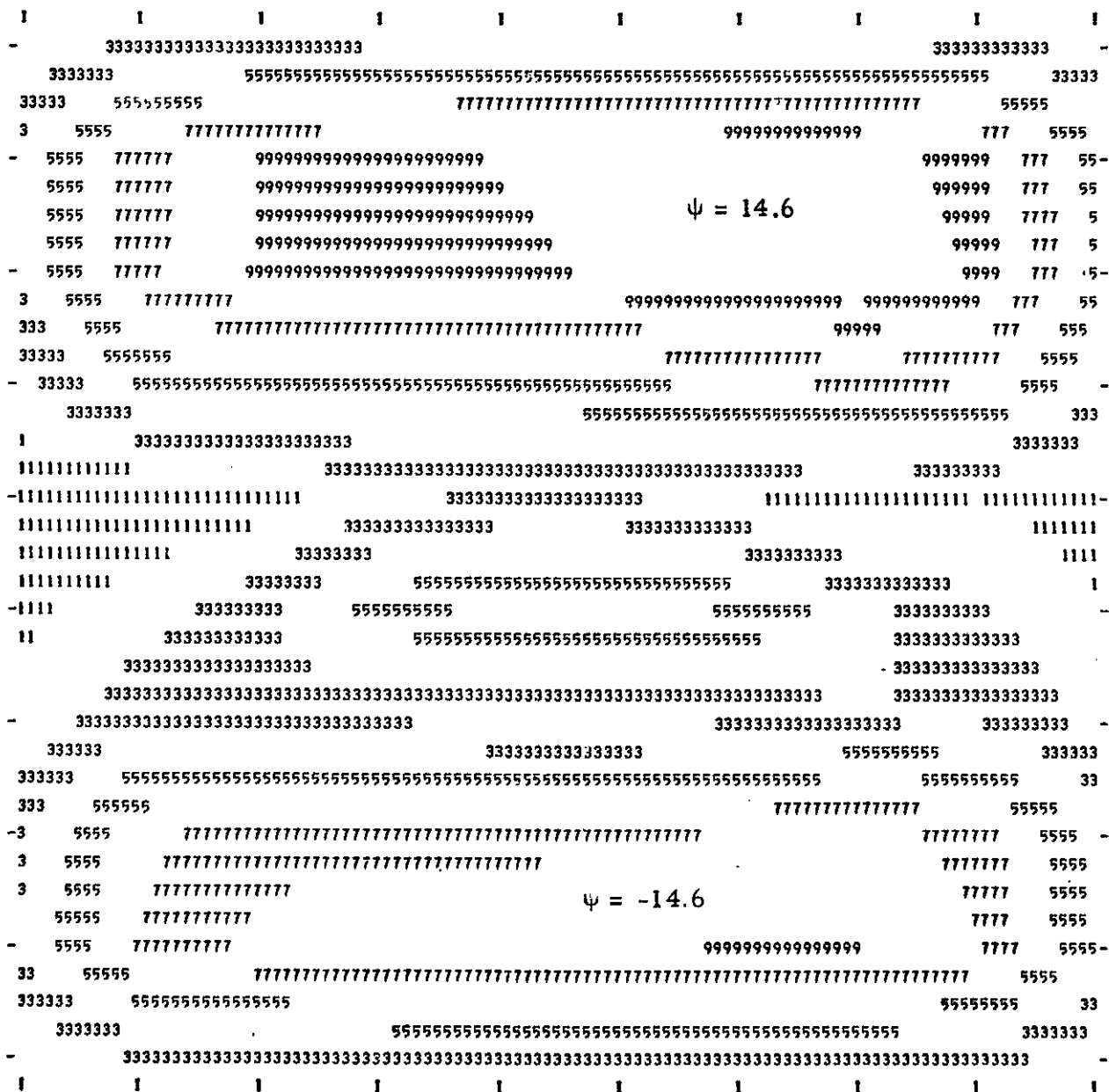


Fig. 10b - Streamline Map for InSb Case I5 (Two Free Surfaces, Ma = 11.7)

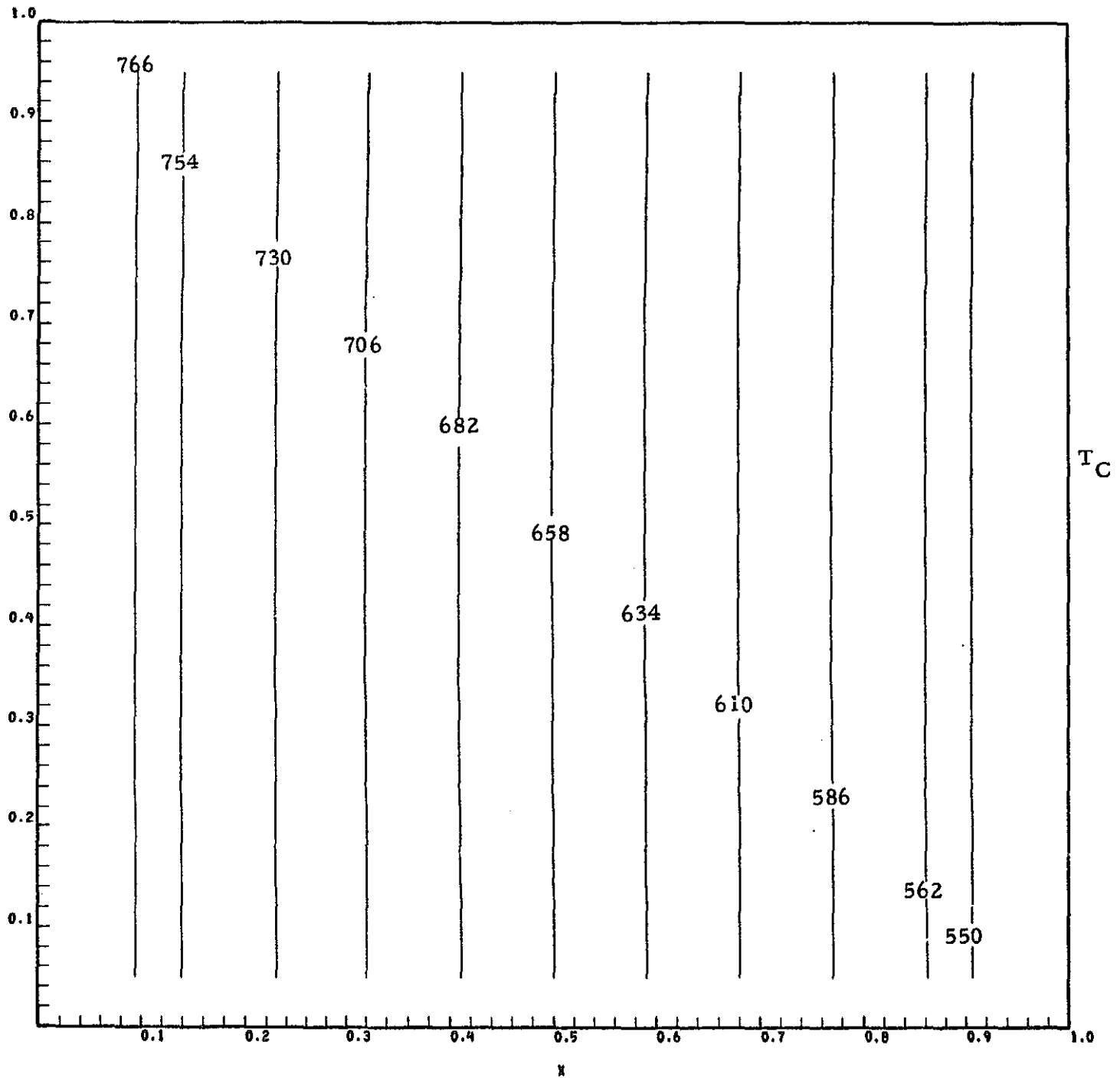


Fig. 10c - Isotherm Maps for InSb Case 15 (Two Free Surfaces, Ma = 11.7)

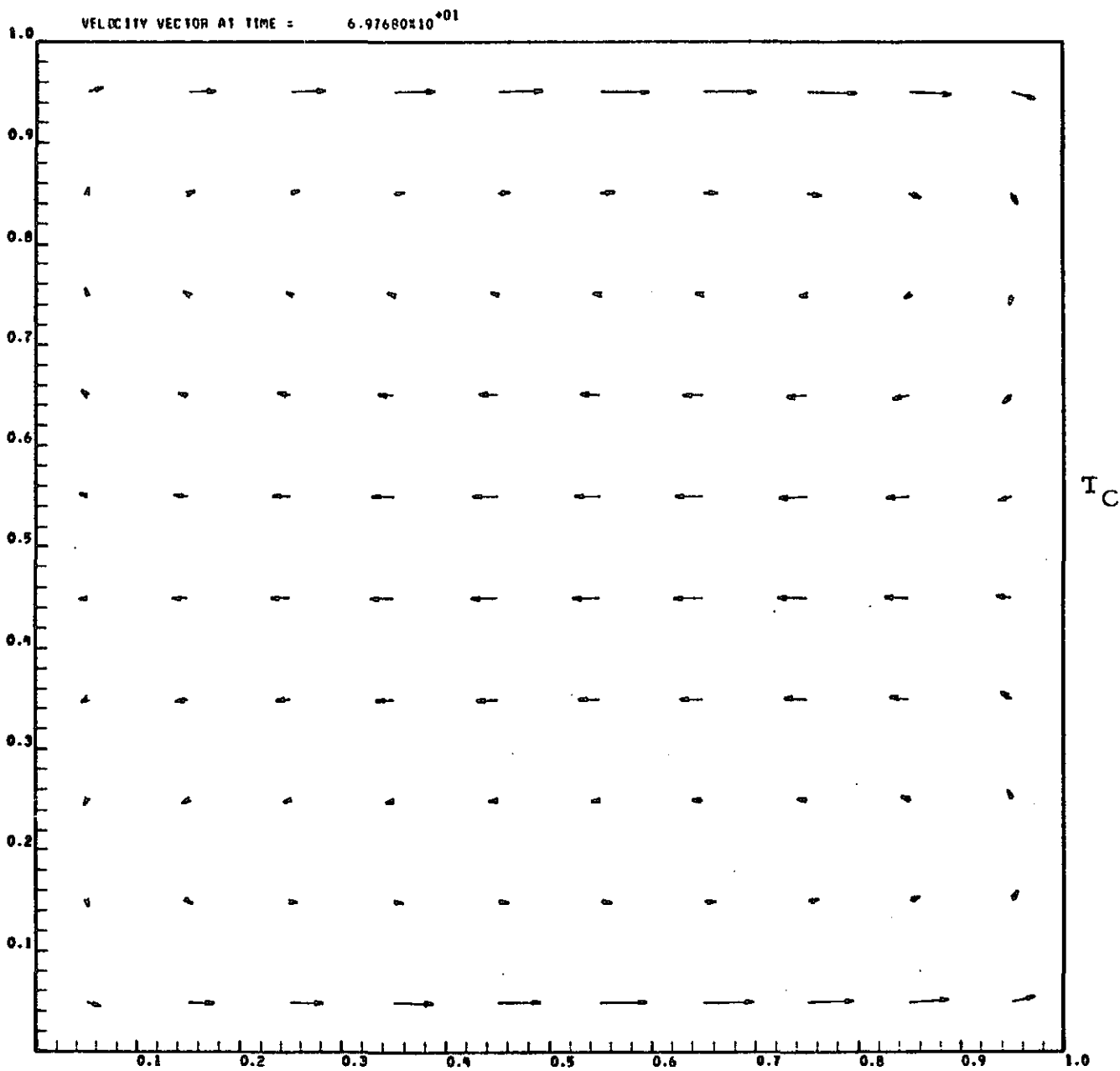


Fig. 11a - Velocity Vector Maps for InSb Case I6 (Two Free Surfaces, $Ma = 117$)

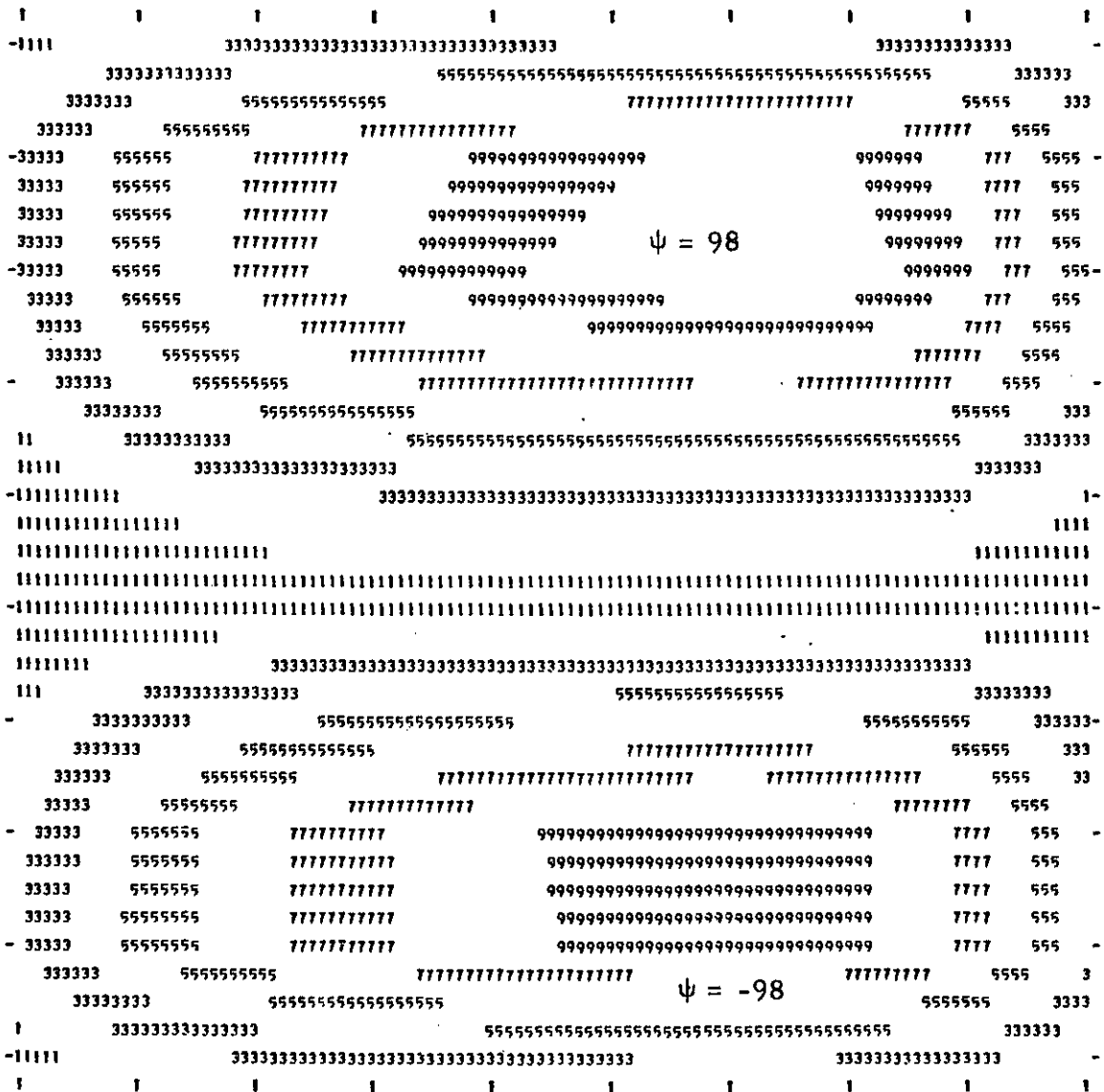


Fig. 11b - Streamline Maps for InSb Case I6 (Two Free Surfaces, $Ma = 117$)

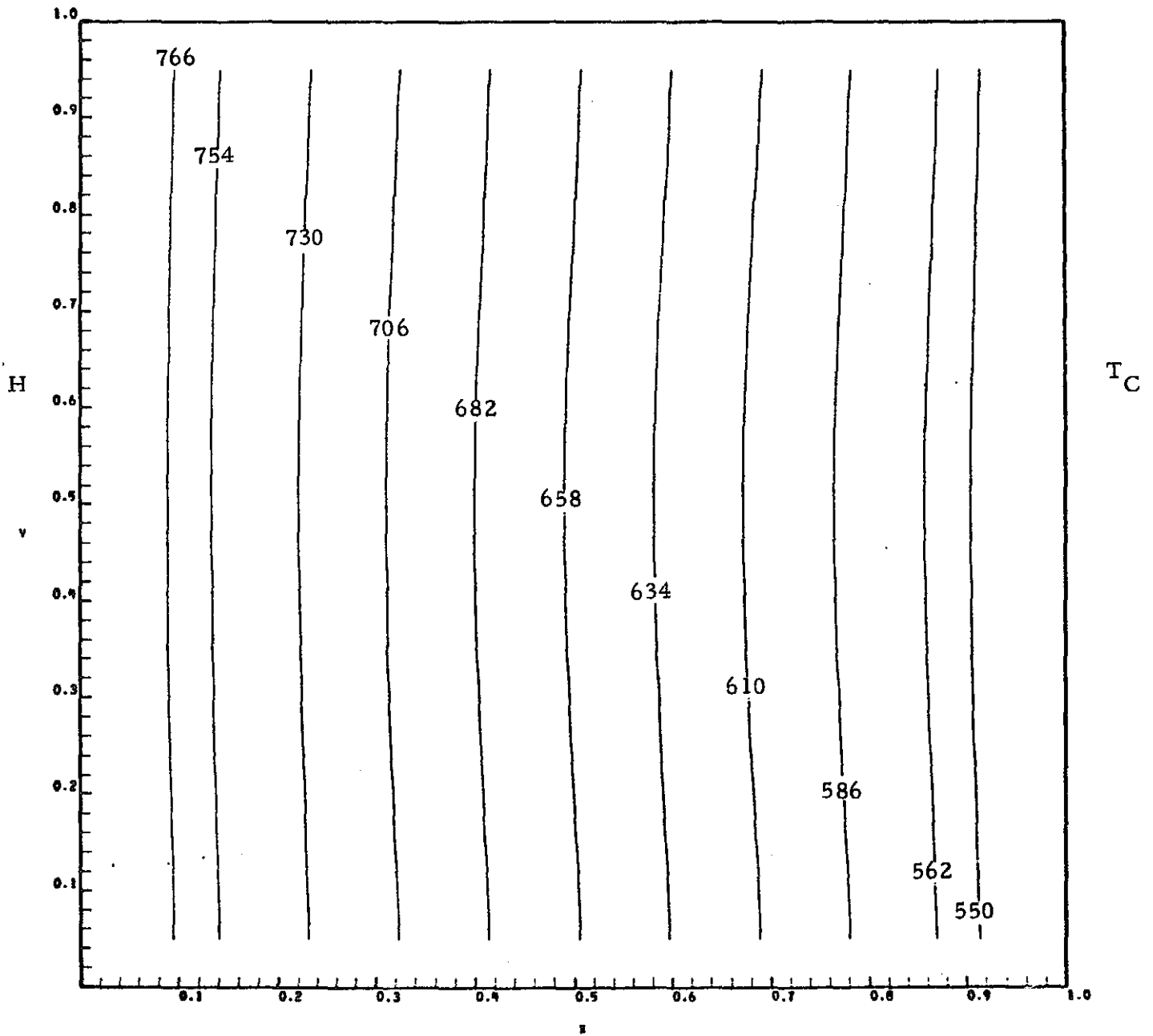


Fig. 11c - Isotherm Maps for InSb Case 16 (Two Free Surfaces, $Ma = 117$)

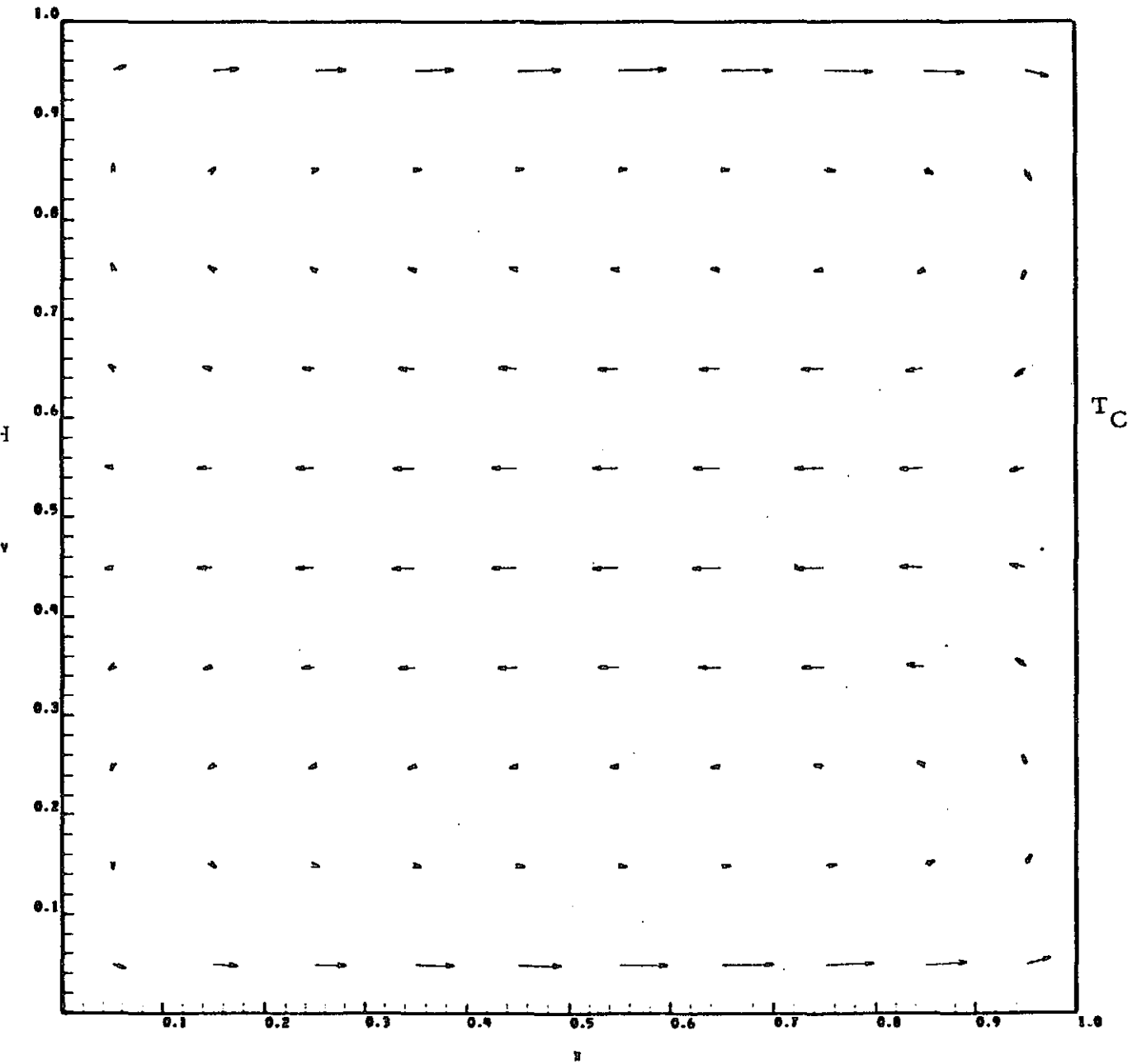


Fig. 12a - Velocity Vector Map for InSb Case I7 (Two Free Surfaces, $Ma = 1170$)

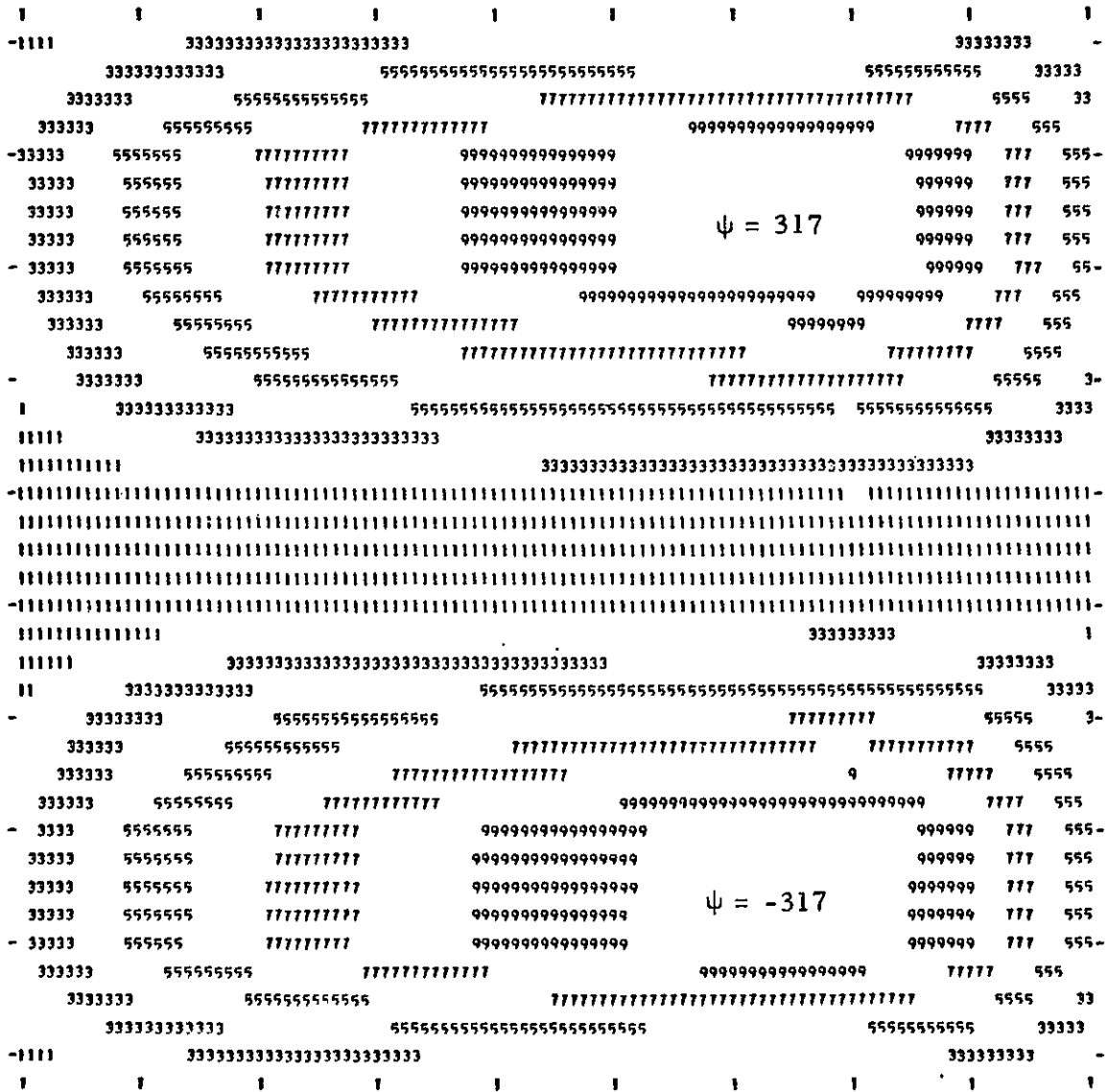


Fig. 12b - Streamline Map for InSb Case I7 (Two Free Surfaces, $Ma = 1170$)

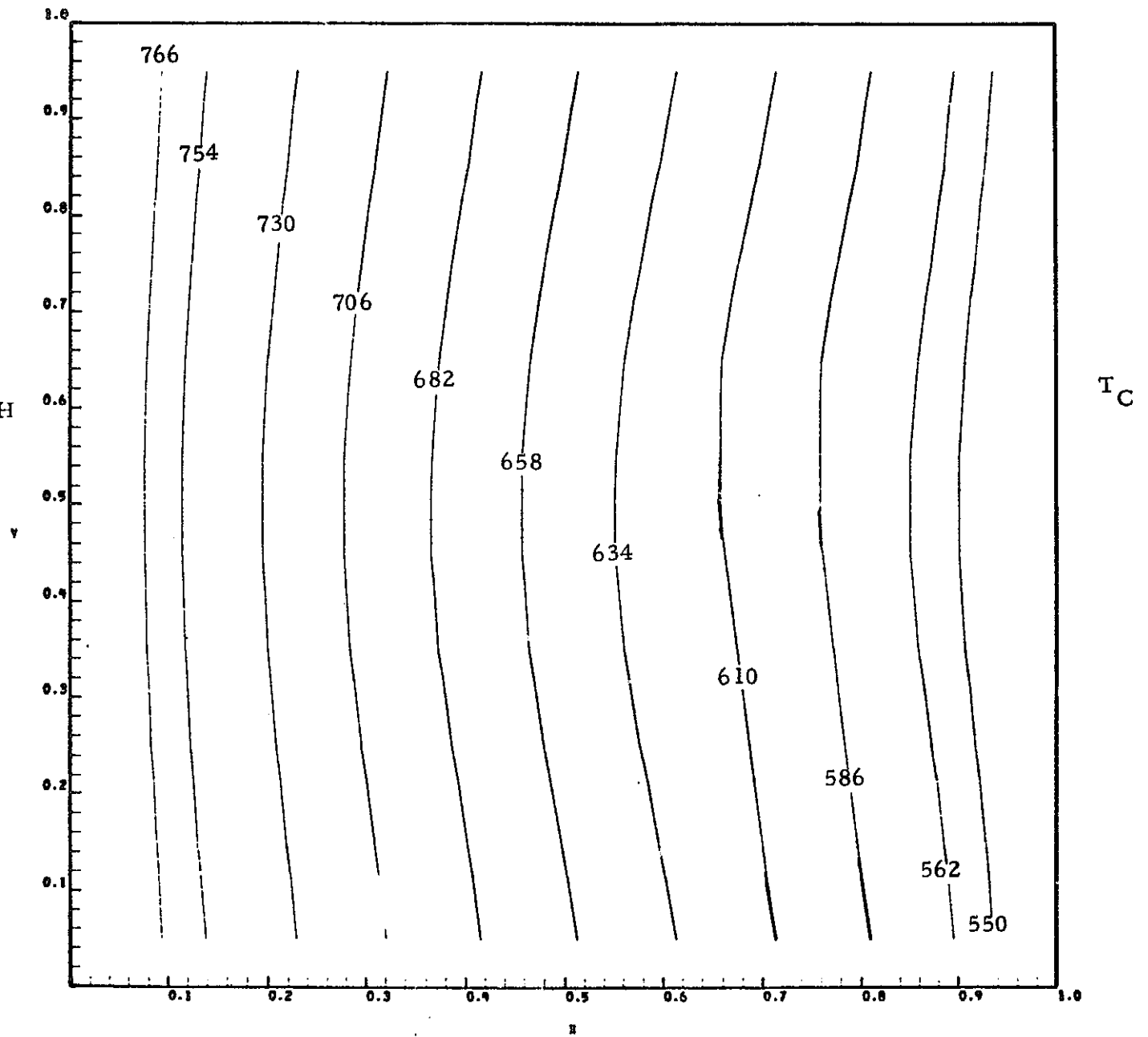


Fig. 12c - Isotherm Maps for IrSb Case 17 (Two Free Surfaces, $Ma = 1170$)

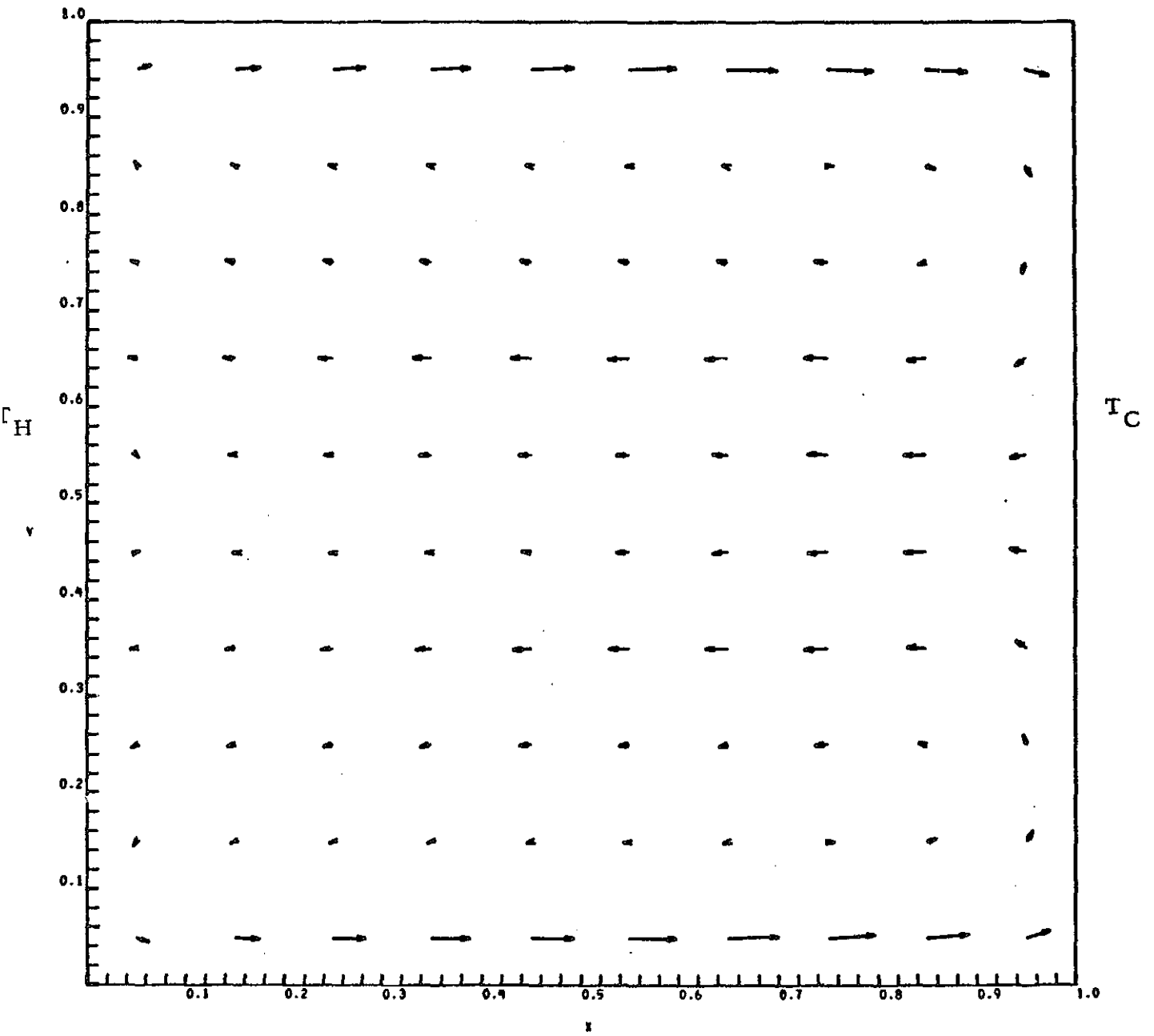
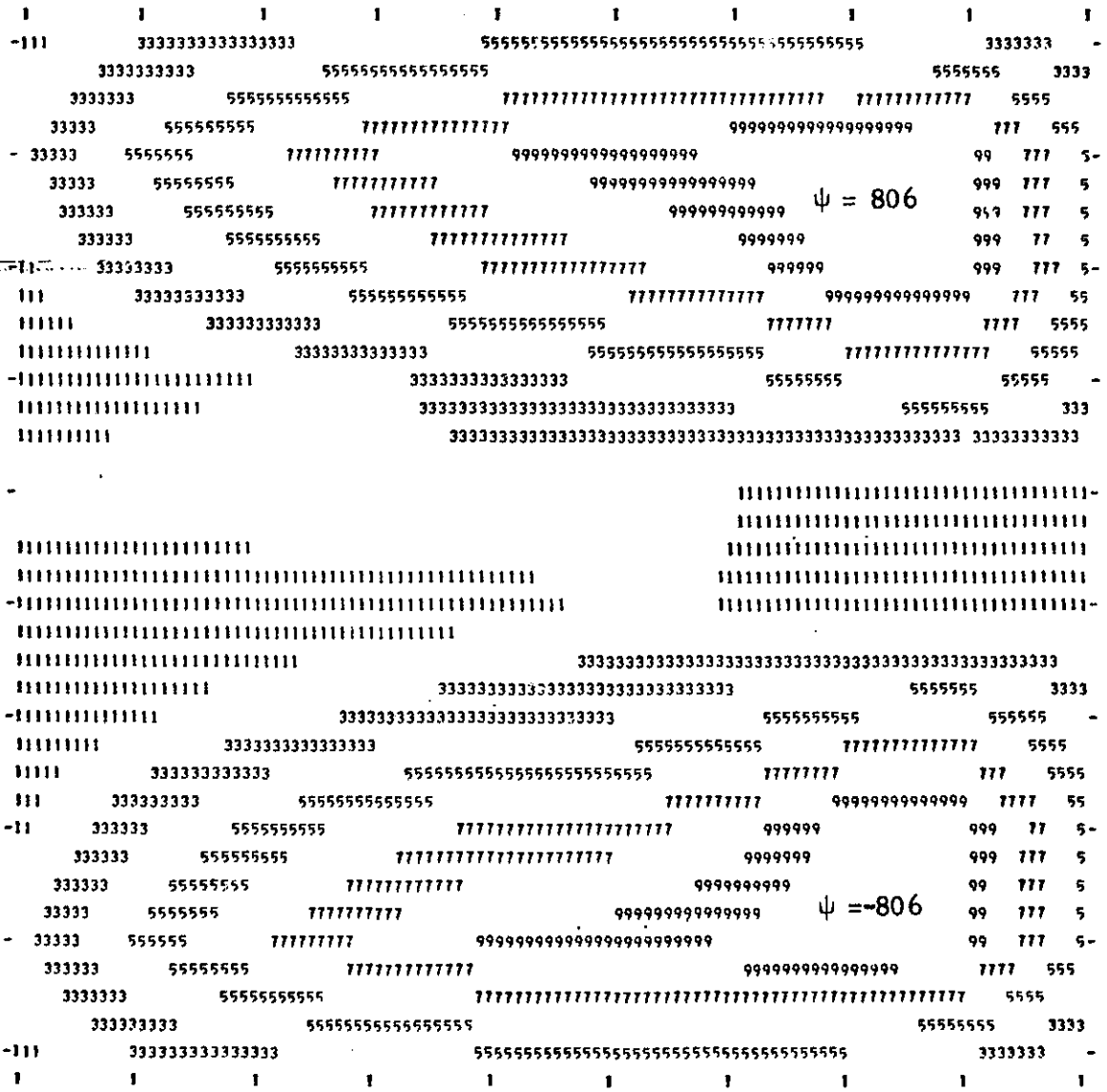


Fig. 13a - Velocity Vector Map for InSe Case 18 (Two Free Surfaces, Ma = 11,700)



T_H

T_C

Fig. 13b - Streamline Maps for InSb Case I8 (Two Free Surfaces, Ma = 11,700)

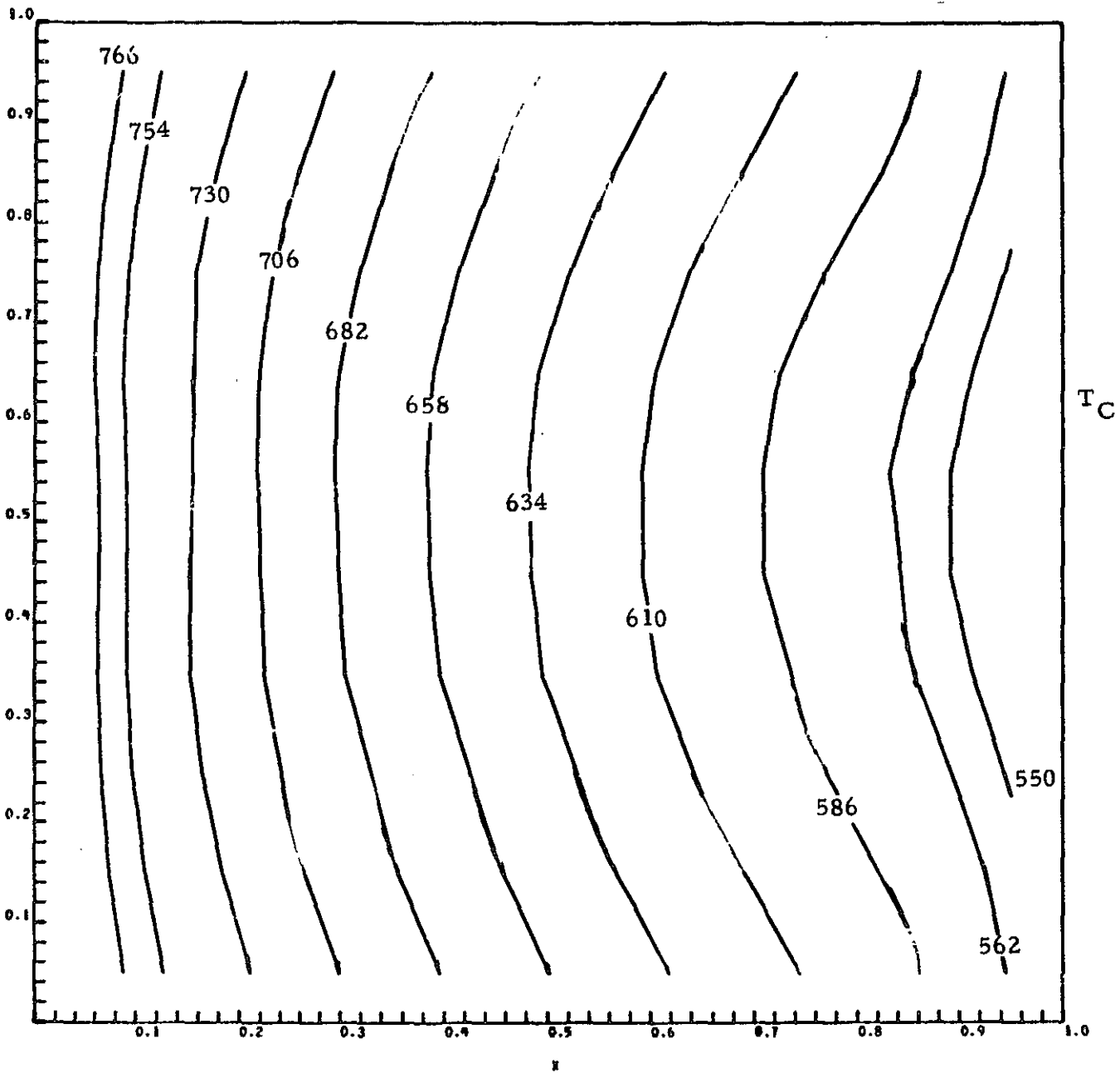


Fig. 13c - Isotherm Maps for InSb case 18 (Two Free Surfaces, $Ma = 11,700$)

Figure 14 is a plot of the calculated mean Nusselt number for the InSb Case 11 (no free surface) versus gravity level. This case was run to determine the g-level at which buoyancy driven convection would influence the M560 experiment. The figure shows that $g = 10^{-1} g_e$ is required to increase the heat transfer by 2% and at 1 g the Nusselt number is only 1.06. This is, of course, due to the large conduction properties of the metal. The curve for $g = 1$ was obtained by extrapolation since the computer runs for this case indicated turbulent flow. We conclude that the acceleration levels aboard Skylab probably did not induce significant buoyant flow.

The data for Nusselt number versus Marangoni numbers given in Table 4 is plotted in Fig. 15 for quick reference and possible extrapolation. It shows that the heat transfer enhancement goes up sharply above Marangoni number of ~ 200 . This curve is valid for low Prandtl number fluids only, since the shear stress boundary condition is a function of Ma/Pr . Higher Prandtl number fluids should produce less heat transfer enhancement for the same value of Marangoni number.

3.5 GERMANIUM CASES

The final computer model case studied consists of the M559 experiment: a container 6.0 cm x 1.4 cm of rectangular cross section which contains liquid germanium. Free surfaces were assumed on the "top" and "bottom" of the fluid along the long dimensions of the container. The boundary conditions were adjusted to produce the largest Marangoni number which would yield laminar flow. This value is $Ma = 19,500$. The results of this case are shown in Fig. 16. The isotherm maps are seen to bend quite drastically due to the 2.61 cm/sec (maximum velocity) flow. The streamline maps show the usual two-cell pattern at the upper and lower walls, but in addition, two "secondary" cells appear to be forming near the left and right walls. This may be realistic or it may indicate that the flow is nearing a turbulent nature. In the latter case, the computer model is not valid.

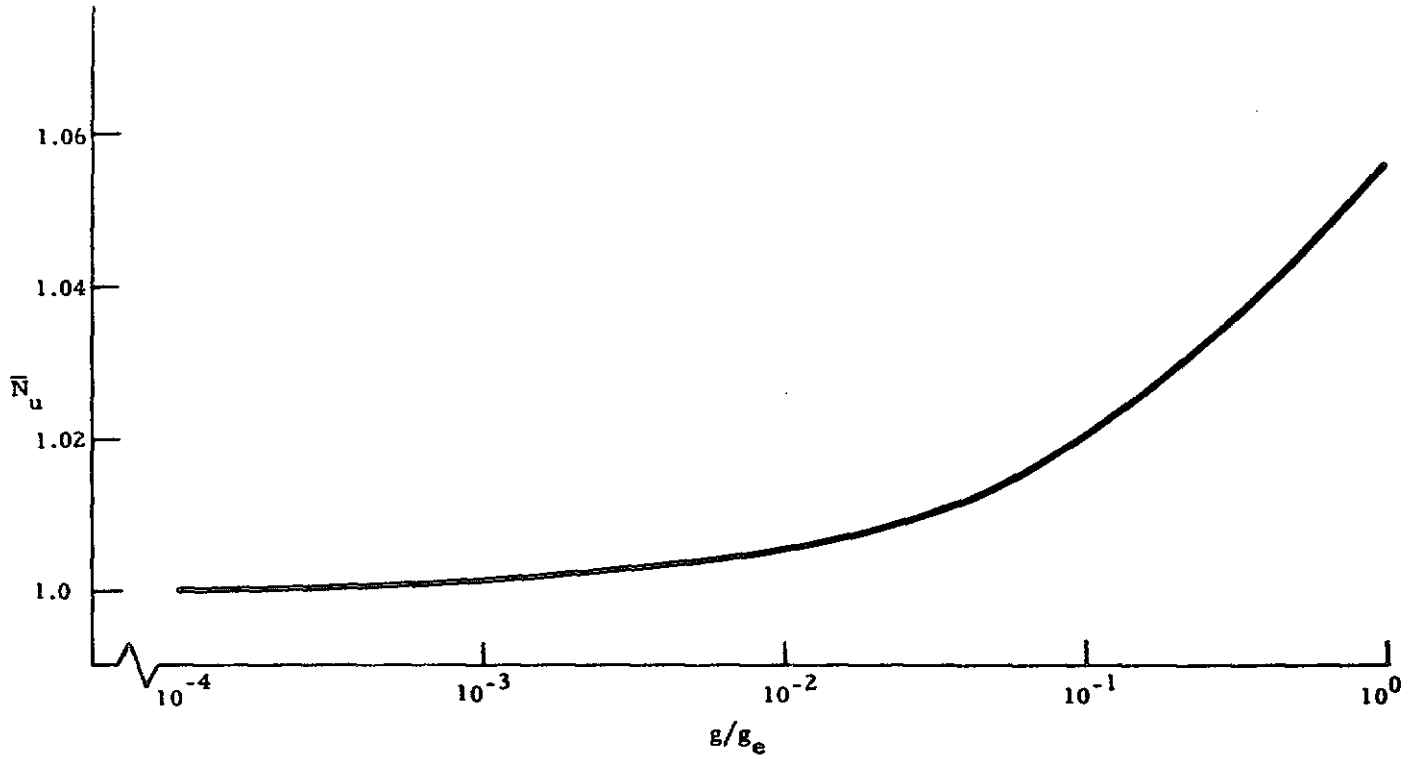


Fig. 14 - Mean Nusselt Number vs g/g_e for InSb Side Heating (No Free Surface) $\eta = 4$

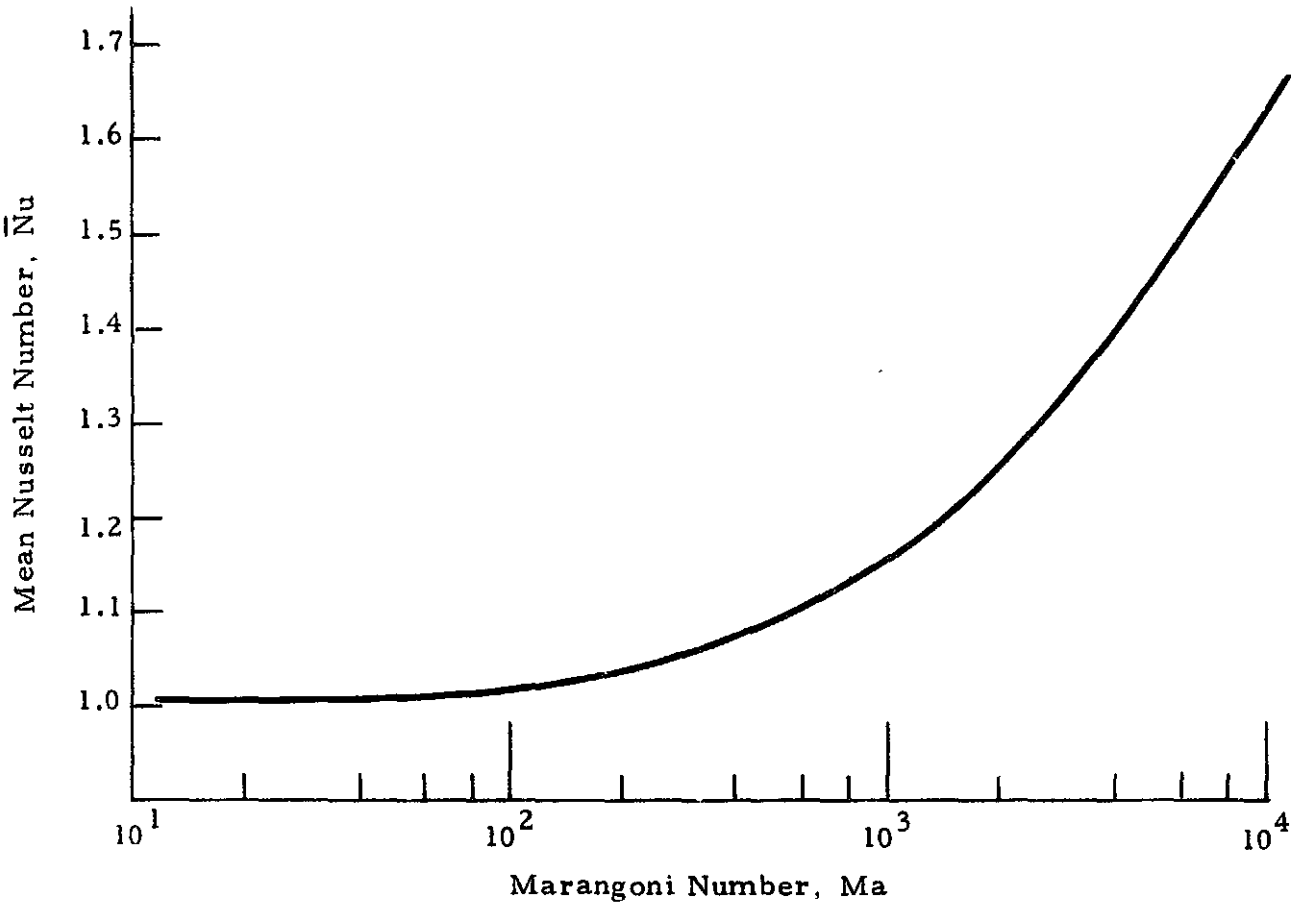
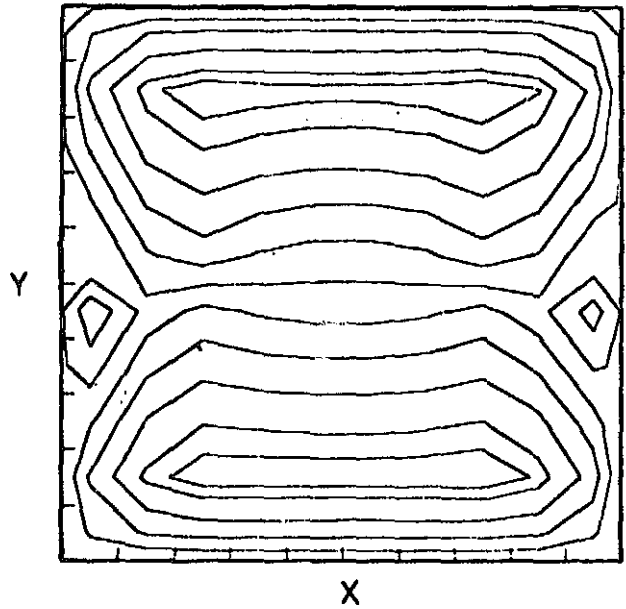
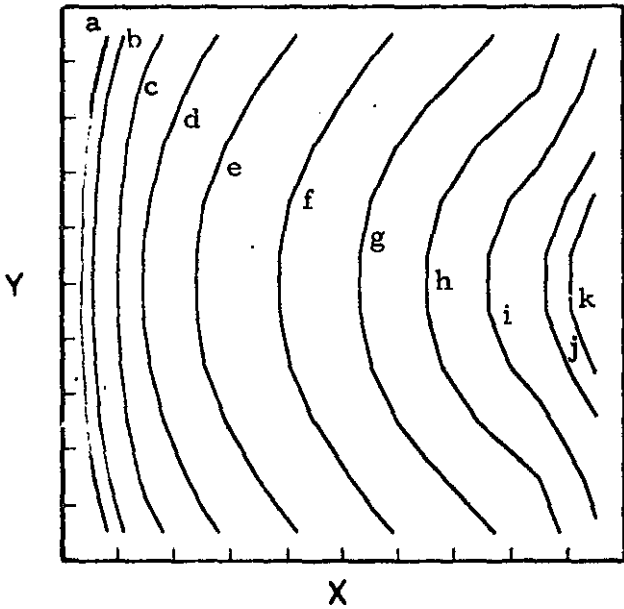


Fig. 15 - Mean Nusselt Number vs Marangoni Number; InSb,
Two Free Surfaces, $g = 0$

ISOTHERMS

STREAMLINES



a. Isotherms

b. Streamlines

a = 766	g = 634
b = 754	h = 610
c = 730	i = 586
d = 706	j = 562
e = 682	k = 550
f = 658	

Fig. 16 - Isotherm and Streamline Maps for Germanium Case, $Ma = 19,507$

The temperature gradient which produces $Ma = 19,500$ is only $2.5 \text{ }^\circ\text{C/cm}$. This case conclusively indicates that if a free germanium surface is present, with even a small temperature gradient along it, then the Marangoni convection could easily approach the turbulent regime. The calculated Nusselt number for this case is $\overline{Nu} = 2.15$ indicating a twofold increase in heat transfer. With $S_c = 10$ for germanium, the mass transfer will be even more significantly augmented. Utilizing Eq. (2.1), $Sh \approx 30$.

3.6 SUMMARY OF CONCLUSIONS

The solutions from the computer program models of convection in the Skylab M556, M559, M560 and M562 experiments have resulted in several conclusions. These are primarily concerned with the conditions which could cause convective flow, the probable magnitudes of the flow and the potential effects on heat and mass transfer processes in the experiments. The conclusions listed below are based on the results of the computer models and are valid within the assumptions made in formulating the models.

- Buoyancy driven convection in the GeI_4 vapor growth experiment is relatively weak in strength; i.e., $\sim 0.014 \text{ cm/sec}$ maximum and more probably $\sim 0.002 \text{ cm/sec}$. This magnitude depends on the orientation of the heating direction with respect to the primary acceleration direction. The exact orientation is apparently unknown.
- The heat transfer rates in the GeI_4 experiment are affected very little by the convective flow; less than 1%.
- The mass transfer in the actual crystal growth should be increased by no more than 20%.
- Buoyancy driven convection in the InSb experiment is also relatively weak; $\sim 0.01 \text{ cm/sec}$ maximum. Because of the high conductivity of the metals, this magnitude of flow causes no appreciable change in the heat transfer.
- A gravity level of $\sim 10^{-1} \text{ g}$ would be required to induce appreciable convective heat transfer in the InSb experiment.

- The possible presence of free liquid surfaces in the InSb experiment is extremely important. The computer model calculations, which are limited to the laminar flow regime, show that velocities of ~ 2.4 cm/sec may result from surface tension driven convection for even moderate Marangoni numbers. This can cause $\sim 67\%$ increase in the steady state rate of heat transfer at the confined walls of the fluid.
- Extrapolations of the laminar models to the full range of surface tension gradients which could exist in the InSb experiment have shown that turbulent flow could easily be generated.
- The effect of having a free surface on both sides of the melt is to reduce the velocity magnitude about 3% for the largest Marangoni number tested.
- The physical properties of germanium produce an even larger potential for Marangoni convection.
- The computer models indicate the temperature oscillations may be setup in the metals experiments if the heating direction is parallel to the primary acceleration direction. No quantitative results were obtained for this orientation.
- The relatively large velocities induced at the free surface can potentially affect mass transfer processes drastically in the metals experiments.

The conclusions reached from this computer model study can be further quantified by refinement of the models themselves. This would require: (1) a better definition of the orientation of the acceleration vector with respect to the container; (2) inclusion of the melting/freezing latent heat effects and the moving solid interface; and (3) in some cases a three-dimensional convection model. The results obtained here are intended to aid the experiment Principal Investigator in analyzing the results of specific Skylab experiments.

Section 4

COMPARISON OF EXPERIMENTAL AND THEORETICAL RESULTS

Experimental data from ground and Skylab processing were limited primarily to crystallographic analyses. The available results are summarized in Refs. 15, 16 and 17 and by recent conversations with the Principal Investigators. Neither thermocouple probes into, nor visual observations of, the melt or gas could be utilized during actual processing. Thus it is very difficult to make direct comparisons between the theoretical results of Section 3 and the available experimental data. Therefore, the following comparisons will be qualitative in nature.

4.1 Ge I₄ EXPERIMENT

Experimental results of Skylab M566 experiment, Case 3A (Ref. 15, p. 241), indicated that an order-of-magnitude increase over expected mass transfer rates was observed. The analysis conducted in Section 3 was performed to investigate if thermogravitational convection could have accounted for this increase. It was shown, as a result of the computer model analysis, that no more than a 20% increase in mass transfer over pure diffusion could be expected by accounting for steady $10^{-3} g_E$ convection, worst-case g-jitter (vibration) convection, and thermoacoustic convection.

The authors thereby conclude that either the measured Skylab mass transfer rates were in error or that the extrapolation of ground based data presented in Ref. 16 were faulty. This could be due to: (1) errors in physical property values for the rather complex system under investigation, and/or (2) to an oversimplified base model for extrapolation (Ref. 16, p. 395). Further ground based testing could provide a proven, correct basis for extrapolating ground tests.

4.2 M560 InSb EXPERIMENT

Experimental results of Skylab M560 indicate that (Ref. 15):

- A. The growth interface maintained a very uniform and slightly convex (to the melt) shape for the majority of its regrowth period.
- B. Regularly occurring transients appeared in the growth rate with a period of ~ 5 minutes which resulted in impurity banding in the crystal.
- C. An axial impurity concentration profile existed in between those typical of classical steady state diffusion controlled and perfect mixing (Ref. 18, p. 332), but more closely resembling diffusion rather than mixing.

Result (A) certainly rules out oscillatory or turbulent convection because these transient modes of convection would induce nonuniformities in the growth interface. In addition, no oscillatory convection modes known exhibit periods of five minutes as in result (B) (see Ref. 19 for thermogravitational and Section 3.4 for thermocapillary). Regarding Result (C), the transient nature of growth under diffusion control or very small convective flows could account for the observed axial impurity profiles.

Thus, it is obvious that the theoretical results of Section 3.4 do not agree with the preceding observed Skylab data. Only the convective results exhibited by $Ma \leq 12$, as exhibited in Fig. 10, could be reconciled with these data. Marangoni numbers this small, however, are two orders of magnitude below those expected. It is not likely that incorporating such effects as actual geometry, impurities or the moving solid/liquid interface would produce such a reduction in convection.

The only plausible explanations are listed below. None of these theories can be proven, however, without further experimental tests. The following reasons for expecting the thermocapillary Marangoni effect to be lowered by orders of magnitude were selected after consultation with recognized experts in surface science and convection (Refs. 20, 21 and 22):

- Oxide Film: Molten InSb, even in the environment of the M560 experiment, is very susceptible to the formation of oxide films. (See Appendix B for details.) Thermodynamics indicate that once such a layer is formed, even if it is only a few angstroms thick, it is virtually impossible to remove (Ref. 21). Thus, the spasmodic breakdown of such a film with a period of five minutes could explain the suppression of Marangoni flow, except for a brief period when the film broke down. The regularity of the film breakup could be due to equipment-induced vibration. Germanium (Experiment M559), on the other hand, is not as susceptible to oxide films in reducing atmospheres such as those on Skylab. Thus turbulent thermocapillary convection could have produced the turbulence seen in M559.
- Counter Concentration Gradients: Concentration gradients may have arisen which would have opposed thermal gradients (e.g., thermocapillary opposed by solutocapillary convection). Concentration gradients should occur due to: (1) Gibbs adsorption of impurities at the vapor/liquid interface is temperature dependent, and (2) segregation of impurities at the growth interface. The lack of physical property data relating to these two phenomena make it impossible to assess their role any further.

Of the two preceding reasons for reduction of capillary convection, it is felt that oxide films are more likely to be the cause. More detailed information concerning the effects of dopants and impurities on liquid metal surface tensions can be found in Appendix C.

4.3 M562 InSb EXPERIMENT

The observed experimental data, the subsequent conflicting theoretical results (Section 3.4), and the rationale for reconciling theory and experiment are practically identical to that presented in Section 4.2. The one significant difference is that the melt was not completely free of the container as in Experiment M560. Thus, one can expect that the many "surface ridges" (Ref. 15) which contacted the container would have lessened the thermocapillary driving forces, but not by several orders of magnitude.

4.4 M559 GERMANIUM EXPERIMENT

Experimental results for the Skylab samples indicated vigorous, turbulent convection (Refs. 15, 21 and 22). This agrees exactly with the predicted theoretical analyses of Section 3.5 and the sensitivity calculations expressed in Table 1. Suppression of convection for germanium can only be obtained in space if free surfaces are eliminated.

Section 5
CONCLUSIONS AND RECOMMENDATIONS

The results presented in Sections 2 through 4 have led to the following conclusions:

- It has been shown that judicious use of both dimensional analysis and an existing computer model (LOCAP) can contribute significantly to post-flight data analysis of the Skylab M518 Multipurpose Furnace crystal growth experiments.
- Neither thermogravitational, g-jitter nor thermoacoustic convection can account for the unexpected, order of magnitude increase in mass transport rate observed in Ge I₄ experiment M556, Skylab Case 3A.
- Turbulent convection existing during Skylab experiment M559, "Microsegregation in Germanium," was definitely caused by thermocapillary forces as predicted from theory both by dimensional analysis and by a convection model.
- From theoretical considerations, both indium-antimonide experiments M560 and M562 should have exhibited substantial thermocapillary convection, but did not due to probable oxide film interference (or opposing solutal effects).

Based on these conclusions and the detailed analyses and information contained in Appendixes B and C, five specific recommendations can be presented:

1. Further ground tests are needed on the GeI₄ M556 experiment to enable accurate extrapolation of mass transfer rates to microgravity conditions. In addition to better physical property and rate measurements, a more rigorous mass transport model upon which to extrapolate from is needed.
2. The effect of temperature, oxide films, dopants and impurities on surface tension of indium-antimonide, and other melts needs to be accurately measured in ground tests.

3. The Lockheed convection computer model should be applied to Skylab experiments:
 - M558 "Radioactive Tracer Diffusion" (Dr. A. O. Ukanwa, Howard University) to determine if the observed radial concentration profiles were caused by Marangoni convection.
 - M563 "Mixed III-IV Crystals" (Dr. W. R. Wilcox, Clarkson Institute of Technology) to determine if the observed sharp radial concentration gradients were caused by Marangoni convection (see Ref. C-3).
 - M566 "Copper Aluminum Eutectic" (E. A. Hasemeyer, MSFC) to decide if lamellae imperfections were caused by Marangoni convection and/or transient growth rates.
4. The Lockheed convection computer model, with the terms accounting for mass transfer, should be applied to Skylab experiments M556, M560 and M562 in order to: (a) more accurately predict mass transfer rates (Eq. (2.1) is just a rough approximation) and (b) provide the radial concentration profiles which result from small Marangoni number ($Ma \leq 12$) flow.
5. Rigorous convection sensitivity and/or convection modeling analyses, in conjunction with measurement or prediction of capillary effects, need to be applied to all space processing flight experiments before final designs are chosen if convection suppression is desired.

REFERENCES

1. Ostrach, S., in "High Speed Aerodynamics and Jet Propulsion," F.K. Moore, ed., Vol. 4, Chapter F, Princeton University Press, Princeton, N. J., 1964.
2. Catton, I., "Effect of Wall Conduction on the Stability of a Fluid in a Rectangular Region Heated from Below," J. Heat Transfer, November 1972, p. 451.
3. Cormack, D. E., L.G. Leal and J. Imberger, "Natural Convection in a Shallow Cavity with Differentially Heated End Walls," J. Fluid Mech., Vol. 65, 1974, p. 227.
4. Chang, C. E., and W. R. Wilcox, "Inhomogeneities Due to Thermocapillary Flow in Floating Zone Melting," J. Crystal Growth, Vol. 28, 1975, pp. 8-12.
5. Layarev, V. B., and M. Y. Dashevskii, "The Surface Tension of Alloys in the System Indium-Antimony, Dokl. Akad. Nauk SSSR, Vol. 146, No. 4, October 1962, pp. 822-825.
6. Pearson, J. R. A., "On Convection Cells Introduced by Surface Tension," J. Fluid Mech., Vol. 4, 1958, p. 489.
7. Carruthers, J. R., "Thermal Convection Instabilities Relevant to Crystal Growth from Liquids," in Preparation and Properties of Solid State Materials, Vol. 2, ed. W. R. Wilcox, Marcel Dekker, New York, 1975.
8. Bird, R., W. Stewart and E. Lightfoot, Transport Phenomena, John Wiley, New York, 1960.
9. Spradley, L. W., and S. W. Churchill, "Pressure and Buoyancy-Driven Thermal Convection in a Rectangular Enclosure," J. Fluid Mech., Vol. 70, Part 4, August 1975, pp. 705-720.
10. Spradley, L. W., and S. V. Bourgeois, "Space Processing Convection Evaluation," AIAA Paper No. 75-695, AIAA 10th Thermophysics Conference, Denver, Colo., 28 May 1975.
11. Spradley, L. W., "Thermoacoustic Convection of Fluids in Low Gravity," AIAA Paper 74-76, January 1974.
12. Spradley, L. W., W. H. Sims and C. Fan, "Thermal Acoustic Oscillations," LMSC-HREC TR D390690-II, Lockheed Missiles & Space Company, Huntsville, Ala., March 1975.
13. Reid, R., and T. Sherwood, The Properties of Gases and Liquids, McGraw-Hill, New York, 1966.

14. Semenchenko, V.K., Surface Phenomena in Metals and Alloys, Pergamon Press, New York, 1961.
15. Proceedings, Third Space Processing Symposium, Marshall Space Flight Center, Huntsville, Ala., 1974 (U.S. Government Printing Office).
16. Wiedemeier, H. et al., "Crystal Growth by Vapor Transport of GeSe, GeSe₂ and GeTe and Transport Mechanism of GeTe," J. Crystal Growth, Vol. 13/14, 1972, pp. 393-396.
17. Witt, A. F. et al., "Crystal Growth and Steady State Segregation Under Zero Gravity: InSb," J. Electrochem. Soc., Vol. 122, 1975, pp. 276-283.
18. Carruthers, J. R., "Crystal Growth from the Melt," in Treatise on Solid State Chemistry, Vol. 5, N. B Hannay, ed., Plenum Press, New York, 1975, pp. 325-406.
19. Carruthers, J. R., "Origins of Convective Temperature Oscillations in Crystal Growth Melts," presented at Third American Conference on Crystal Growth, Stanford University, 13 July 1975.
20. Scriven, L. E., Private Communication, 19 September 1975.
21. Wilcox, W. R., Private Communication, 19 September 1975.
22. Carruthers, J. R., Private Communication, July 1975.

NOMENCLATURE

<u>Symbol</u>	<u>Definition</u>
C_p	heat capacity of liquids, cal/g
D	diameter of container, cm
g	dimensionless gravity level (gravity/earth gravity)
g_E	earth gravity, 980 cm/sec ²
Gr	Grashof number
k	thermal conductivity of liquid, cal/cm-sec-°C
L	length or height of container, cm
Nu	Nusselt number, total heat transfer/conduction
P	pressure
Pr	Prandtl number, $\mu C_p/k$
r	radial coordinate of container, cm
R	radius of container, cm
Ra	Rayleigh number, $\rho^2 C_p \beta g \Delta T L^3 / \mu k$
T	temperature, °C
u	radial or lateral component of velocity in the fluid, cm/sec
v	axial or vertical component of velocity in the fluid, cm/sec
W	width of container, cm
x,y	Cartesian coordinates, cm
z	axial coordinate of container, cm

<u>Greek</u>	<u>Definition</u>
α	thermal diffusivity, cm^2/sec
β	coefficient of thermal expansion, $1/^\circ\text{C}$
γ	aspect ratio of container (height-to-diameter)
μ	viscosity, $\text{g}/\text{cm sec}$
η	aspect ratio of container (width-to-height)
ρ	density, g/cm^3
ν	kinematic viscosity, cm^2/sec
ψ	stream function, cm^2/sec

Appendix A
DESCRIPTION OF LOCKHEED CONVECTION
ANALYSIS PROGRAM

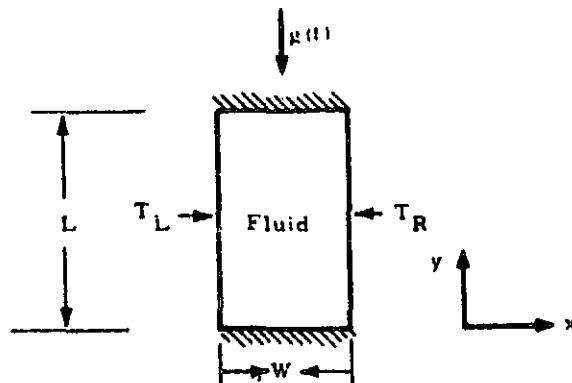
PRECEDING PAGE BLANK NOT FILMED

Appendix A

LOCKHEED CONVECTION ANALYSIS PROGRAM -- LOCAP

The study of convection in the Skylab experiments was performed by utilizing the Lockheed Convection Analysis computer program (LOCAP). LOCAP is a general purpose digital computer code for natural convection analysis. Among the capabilities of the program are: (1) rectangular or cylindrical geometries; (2) gases or liquids; (3) transient and steady state analysis; (4) confined fluids and free surface flows; (5) time-varying body force; (6) temperature-dependent material properties; (7) heating from the side or from below; (8) combinations of heat flux and temperature boundary conditions; and (9) two-dimensional or axisymmetric laminar flow. A complete formulation of the various models utilized by the program is given in Refs. 9 through 12.

A typical formulation is now given for a problem using a rectangular geometry and Cartesian coordinates. This is presented for the reader interested in how the math model is constructed. The sketch below shows the geometry, coordinate system and configuration of the model. A rectangular



Coordinate System and Boundary Conditions (Typical Configuration)

box of width, W , and length, L , confines a fluid between rigid boundaries. The fluid can be initially at rest and isothermal. The gravitational acceleration is time-dependent and in the direction of the $-y$ axis. As the left wall is heated, flow is initiated by buoyancy due to density gradients. The problem now consists of determining the flow characteristics and heat transfer as a function of time or until a steady state is reached.

The mathematical formulation of the problem is in terms of the Navier-Stokes equations in primitive variable form. Assumptions made in this illustrative case are: (1) material properties except density are constant; (2) laminar flow of a Newtonian fluid; (3) viscous effects in the momentum equation are for incompressible flow; (4) viscous dissipation, radiation and compressibility are neglected in the energy equation. The governing equations are given below in terms of dimensionless variables and in conservation law form.

X-Momentum

$$\frac{\partial}{\partial t} (\rho u) + \frac{\partial}{\partial x} (\rho u^2) + \eta \frac{\partial}{\partial y} (\rho uv) = - \frac{\partial P}{\partial x} + \left(\frac{\partial^2 u}{\partial x^2} + \eta^2 \frac{\partial^2 u}{\partial y^2} \right)$$

Y-Momentum

$$\frac{\partial}{\partial t} (\rho v) + \frac{\partial}{\partial x} (\rho uv) + \eta \frac{\partial}{\partial y} (\rho v^2) = \bar{G}(\rho-1)g - \eta \frac{\partial P}{\partial y} + \left(\frac{\partial^2 v}{\partial x^2} + \eta^2 \frac{\partial^2 v}{\partial y^2} \right)$$

Continuity

$$\frac{\partial \rho}{\partial t} + \frac{\partial}{\partial x} (\rho u) + \eta \frac{\partial}{\partial y} (\rho v) = 0$$

Energy

$$\frac{\partial}{\partial t} (\rho T) + \frac{\partial}{\partial x} (\rho u T) + \eta \frac{\partial}{\partial y} (\rho v T) = \frac{1}{Pr} \left(\frac{\partial^2 T}{\partial x^2} + \eta^2 \frac{\partial^2 T}{\partial y^2} \right)$$

State Relation

$$\beta \Delta T + \frac{\Delta \rho}{\rho} - K \Delta P = 0$$

Where the dimensionless groups are:

$$\begin{aligned} \eta &= W/L && \text{Aspect ratio} \\ \bar{G} &= -\frac{\bar{g}_E}{g_E} W^3/\nu^2 && \text{Buoyancy parameter (similar to Grashof number)} \\ Pr &= \mu C_p/k && \text{Prandtl number} \\ \beta &= -1/\rho_o (\partial \rho / \partial T)_P && \text{Coefficient of thermal expansion} \\ K &= 1/\rho_o (\partial \rho / \partial P)_T && \text{Coefficient of isothermal compressibility} \end{aligned}$$

Boundary conditions for the equations can be various combinations of wall heat fluxes, temperatures, no slip, free slip and free surface conditions. A simplified set are the following:

Typical Initial Conditions

$$\begin{aligned} u &= v = 0 \\ T &= 1 \\ \rho &= 1 \\ T &= 1 \end{aligned}$$

Typical Boundary Conditions

$$\begin{aligned} u &= v = 0 && \text{at solid walls} \\ T(x=0, y) &= T_L \\ T(x=1, y) &= T_R \\ \partial T / \partial y &= 0 && \text{at } y = 0 \\ \partial T / \partial y &= 0 && \text{at } y = 1 \end{aligned}$$

A finite difference method is used for obtaining numerical solutions to the equations. The basic method is that of Spradley and Churchill (Ref. 9). It utilizes an explicit finite difference, forward-marching method. Centered differences are used for all terms except the convection terms where a conservative donor method is applied. The grid consists of a sequence of cell-centered points with the spacings Δx , Δy constant but not necessarily equal. The utility of the method is that it yields both transient and steady state solutions, is conditionally stable and numerically conservative.

The solution process begins at some time where a flow field is known. This can be $t = 0$ with the fluid isothermal and at rest or at $t = t_f$ where the flow field is supplied from the solutions for a previous case. The flow for "heating-from-below" cases is initiated by either a temperature perturbation from the conductive state or by using the flow from a previous case. From the initial data the equations are solved to march the solution forward in time to yield the velocity components, density and temperature profiles at all grid points in the container. The solutions are mapped as isotherm contours, streamlines and/or velocity vector fields. The LOCAP code, the numerical technique and solution algorithms have been verified for many sample problems by comparing them with previous theory and experimental data (Refs. 9 through 12). The program is in production status for use on a Univac 1108 multiprocessor computer system.

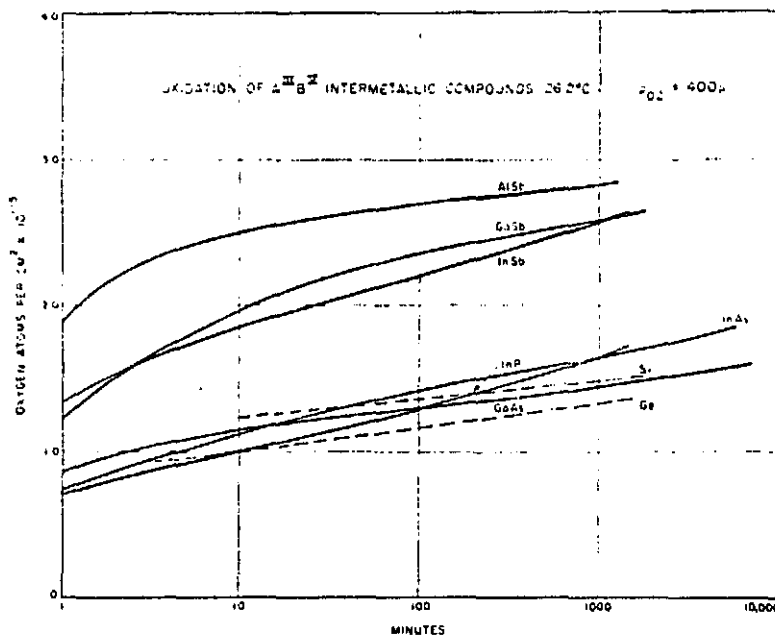
Appendix B^{*}
InSb OXIDE FILMS

^{*}Contributed by J. P. Doty.

Appendix B

Indium antimonide which is exposed to air at room temperature will very readily form an oxide coating on its surface. Measurements by A. J. Rosenberg* have been made on the oxidation rate of InSb at 400 microns of oxygen pressure at a temperature of 26.2°C.

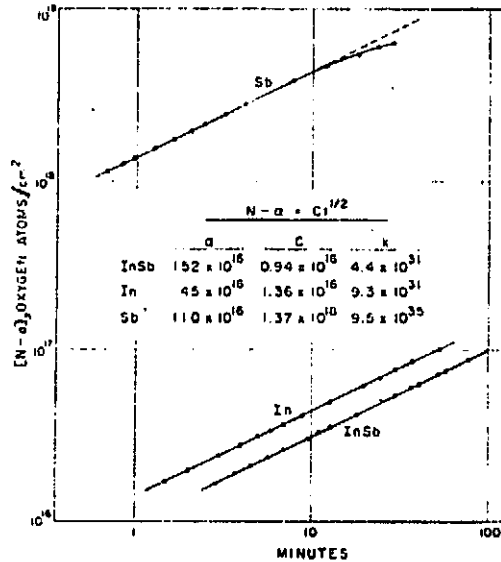
These measurements along with oxidation rates of other III-V compounds are shown in the following figure.



Oxidation of III-V compounds at 26.2°C. $p_{O_2} = 400$ microns
(After Rosenberg)

*Rosenberg, Arthur J., "The Reactions of III-V Intermetallic Compounds with Gaseous Oxygen," Vol. 1, Chapter 49 of Compound Semiconductors, Edited by R.K. Willardson and H. L. Goering.

This figure shows a quantity of oxidation of 6% that of the quantity at 367°C. This can be seen by comparing the figure on page B-1 with the figure immediately below.



Comparison of oxidation rates of indium, antimony, and InSb at 367°C (after Rosenberg and Lavine). The data are normalized to unit surface area using a roughness factor of 1.3 for InSb, and the cross sectional area of the sample tube for indium. Unit roughness factor is assumed for antimony which was obtained by cleavage.

These reactions are irreversible and once a sample of InSb is exposed to air an oxide coating will be present.

In the M560 experiment, the sample was prepared and was probably exposed to air prior to placing in the quartz tube to be evacuated and sealed off. During this time an oxide coating would have built up on the exposed surface. Thus, it is almost a certainty that the sample had an oxide film on its surface after being sealed into the ampoule.

The ampoule was fitted to 350 torr with ultrahigh purity hydrogen prior to sealing which would stop any further oxidation of the surface. Upon heating the ampoule to melt temperature, much of the oxide film would react with the hydrogen. The amount of oxide film remaining would be directly proportional

to the quantity of hydrogen and to the quantity of oxygen on the sample surface when sealed in the ampoule. This quantity of oxide film is a direct function of the time the sample was exposed to air prior to being sealed in the ampoule.

Thus, unless the sample was exposed to air only a few seconds or less, an oxide film could exist on the sample after melting and crystal growth. This oxide film may only be one or a few atomic layers thick, but it is very probably present on the grown crystal.

Appendix C
DOPANT EFFECTS ON MELT-VAPOR SURFACE TENSION

Appendix C

Liquid metals possess unusual and/or ill-defined interfacial phenomena because (Ref. C-1):

- Liquid metals are notable for their high surface tensions; typical values in the presence of inactive gases are listed in Table C-1. These may be compared with 72 dyne cm^{-1} for water at 20°C and values ranging from 17 to 45 dyne cm^{-1} for most organic liquids.
- Many solutes in liquid metals are surface active, especially oxygen, sulphur, selenium and tellurium. The effects of these on the surface tension of copper are shown in Fig. C-1. Because many non-metals are highly surface active, reported values of surface tension are open to doubt, unless special precautions have been taken to eliminate impurities. Solute metals are generally less surface active than non-metals. In the case of iron those listed in Table C-2 have substantial effects but they are much less active than O, S, Se and Te.
- The effect of temperature is to lower the surface tensions of pure metals but to raise the surface tensions of solutions in which the surface tension is markedly lowered by a surface-active substance. Thus the curves of surface tension versus composition typically change with temperature as shown in Fig. C-2 for solutions of Te in Sn.

From Fig. C-2, it is obvious that $d\sigma/dT = 0$ for certain concentrations of Te. If such a concentration existed for the Te-doped M562 experiment, thermocapillary convection would have been suppressed. Similar effects by Se could have occurred in the M560 experiment.

Influence of Two Solutes

In general, the effects of two solutes together cannot be predicted. The surface tensions of steels cannot be calculated from their compositions even approximately, because the effects of sulphur and oxygen together are not additive, and their behavior is affected in unpredictable ways by alloying elements. Also, two non-active solutes when present together may produce

Table C-1
SURFACE TENSIONS OF LIQUID METALS

Group	Metal	Temp. (°C)	Surface tension (dyne cm ⁻¹)
1b	Cu	1120	1280
1b	Ag	970	920
1b	Au	1070	1127
2b	Zn	420	750
2b	Cd	330	550
2b	Hg	20	465
3b	Ga	30	725
3b	In	160	340
3b	Te	450	460
4	Si	1420	~725
4a	Ti	~1670	1510
4b	Sn	~240	~550
4b	Pb	400	445
5b	Sb	640	395
5b	Bi	400	375
6a	Cr	1540	> 1590
6a	W	3380	2310
7a	Mn	~1250	> 1300
8	Fe	1550	1788
8	Co	1550	1896
8	Ni	1550	1934
8	Pt	1800	1699

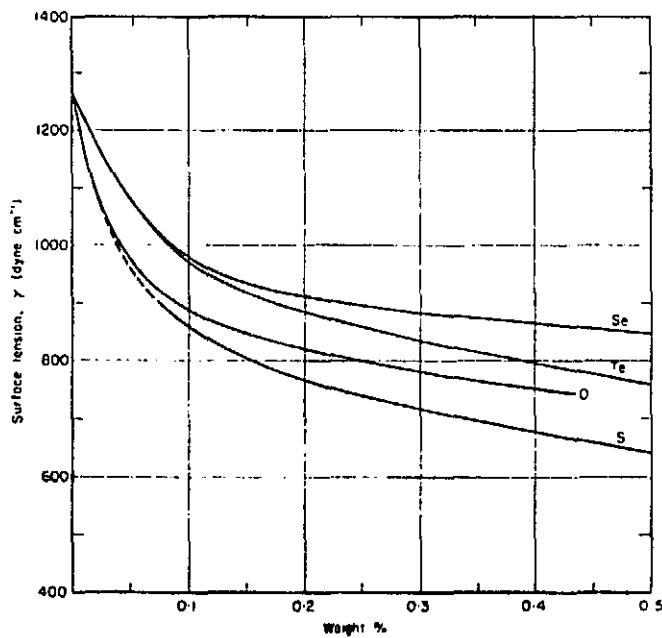


Fig. C-1 - Surface Tensions for Solutions O, S, Se, Te, in Liquid Copper at 1150°C (Ref. C-1)

Table C-2

dy/d (ATOM % SOLUTE) FOR VARIOUS SOLUTES IN LIQUID IRON, AND NICKEL (WITH ASTERISK) (REF. C-2)

Group in Periodic Table	3	4	5	6
Element	B ~ 26 Al ~ 38 In* ~ 1800	C ~ 3 Si ~ 6 Sn ~ 1600 Sn* ~ 1000	N 850 P 13 As ~ 200 Sb ~ 3900	O 8,600 S 15,400 Se 54,600 Te > 54,600

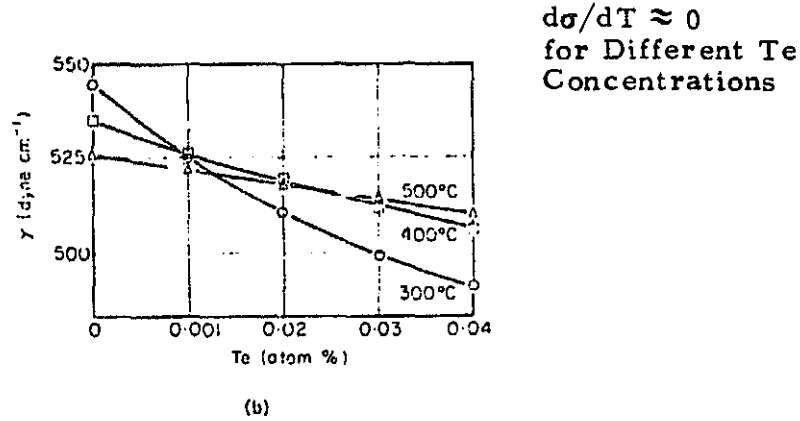


Fig. C-2 - The Surface Tensions of Solutions of Te in Liquid Sn at Three Different Temperatures (Ref. C-2)

a surface-active soluble compound. For example, chromium and carbon are both inactive in liquid iron, but when present together at concentrations too low for the formation of free carbides, the surface tension is markedly lowered. A similar situation arises with iron containing tungsten and carbon together. Surprisingly there are no such effects when vanadium and nitrogen or chromium and nitrogen are present together, in spite of the tendency for these metals to form stable nitrides.

Thus, only careful measurements of the melt-vapor systems utilized in the M518 experiments would enable rigorous diagnostics to be performed for these experiments regarding capillary effects.

Kinetics of Adsorption

From the preceding discussions, it is likely that Te, Se, and other solutes will preferentially absorb at the melt-vapor interface. It is possible to apply the Gibbs adsorption equation to solutes in liquid metals in order to estimate the excess of solute in the surface region over and above the concentration in the bulk liquid.

Considering the time required for an adsorbed solute to make its way by diffusion from static bulk liquid to a fresh surface, one can write (see Eq. (11.34) Ref. C-1),

$$\dot{n} = \left(\frac{D}{\pi t} \right)^{1/2} \Delta C,$$

where ΔC is the driving force for adsorption in terms of concentration. At the commencement of adsorption ΔC is virtually equal to the concentration in the bulk liquid, but it decreases in a complex manner as adsorption proceeds. For an order of magnitude calculation, ΔC can be taken as constant,

$$n = 2(D/\pi)^{1/2} t^{1/2} C .$$

Utilizing D of $5 \times 10^{-5} \text{ cm}^2 \text{ s}^{-1}$, typical of oxygen in iron, n equal to the surface excess $18 \times 10^{-10} \text{ mole cm}^{-2}$ and C equal to 7×10^{-5} (oxygen at 0.016 wt%), t becomes about 10^{-5} s . Because of the fall in driving force as adsorption proceeds, the actual time is about some four or five times as great. Nevertheless the surface concentration is established almost instantaneously even when the bulk oxygen concentration is less than one tenth its saturation concentration.

These calculations indicate that the M518 experiment's surface active materials such as O, Te, and Se would have saturated the L/V interface in seconds.

Nature of the Surface Layer

It seems almost certain that melt surfaces are packed with negatively charged anions and that immediately beneath them lie positively charged metal atoms. There may thus be an electrical double layer which becomes less and less ionic as the polarizability of the solute increases through sulphur to selenium and tellurium.

Ground Evidence of Melt Marangoni Stirring

An interesting case of surface flow, arising from surface tension differences set up in a gas-metal reaction, is illustrated in Ref. C-1, p. 453. A small jet of oxygen is being directed at the center of the top surface of unstirred liquid tin contained in a small crucible at 1190°C . Directly beneath the jet, tin oxide is produced and this looks bright because of its high emissivity. Because the oxide wets the metal and has a much lower surface tension than the unoxidized tin, which is at a distance from the jet, it has a high spreading coefficient. Thus the oxide is drawn out towards the sides of the crucible in streaks, dissolving rapidly as it moves. In addition the metal near the oxide, which is high in oxygen, probably has a much lower surface tension than the metal near the walls, so that a radial flow of metal is induced towards the sides of the crucible from the center. The net result is radial movement of oxide and

metal with velocities which range up to 150 cm s^{-1} in a 4.5 diameter crucible. It has been shown that this movement is not attributable to the momentum of the gas emerging from the jet.

Conclusions

Little data exist on capillary convection in molten metals or on the effects of dopants and impurities on interfacial tensions. The data presented in this appendix however, illustrate that solutal effects (from such highly surface-active solutes as O, Se, Te) could have accounted for the apparent suppression of thermocapillary convection in Skylab experiments M560 and M562, versus the presence of significant capillary-driven convection in Skylab experiments M559 and M563 (Ref. C-3).

References

- C-1. Richardson, F.D., Physical Chemistry of Melts in Metallurgy, Vol. 2, Academic Press, New York, 1974, pp. 426-461.
- C-2. Kozakevitch, P., in Surface Phenomena of Metals, Society of Chemical Industry Monograph 28, 1968, p. 223.
- C-3. Lefever, R.A., Monthly Progress Report, Contract NAS8-28305, University of Southern California, Los Angeles, 15 September 1975.